Adaptive Finite-Time Control Scheme for Teleoperation With Time-Varying Delay and Uncertainties

Haochen Zhang, Aiguo Song, *Senior Member, IEEE*, Huijun Li, Dapeng Chen, *Member, IEEE*, and Liqiang Fan

***Abstract*—The communication time delay and uncertain models of robotic manipulators are the major problem in the teleoperation system, which can reduce the performance and stability of the system. This article proposed a novel finite-time adaptive control scheme for position and force tracking performances of the teleoperation system. First, a combined auxiliary error system with position and force tracking errors is designed. Second, a velocity feedback filter is introduced, and a new auxiliary variable function with finite-time structure is designed for controller design. The radial basis function neural network (RBFNN) is applied to estimate the uncertain parts. Then the finite-time adaptive control scheme and adaptive laws are given. Third, based on the Lyapunov method, stability and finite-time performance are demonstrated. And finally, the simulation and experimental studies (with Phantom Ommi devices) are performed and demonstrate the effectiveness of the proposed control scheme on teleoperation position/force tracking.**

***Index Terms*—Adaptive control, communication delay, finite-time control, position/force tracking, teleoperation.**

I. Introduction

SINCE the first teleoperation system was applied to grab the nuclear materials for more than 70 years, the teleoperation robots have been widely employed in many fields, such as space operation [1], deep-sea exploration [2], remote surgery [3], medical rehabilitation [4], handling dangerous substances [5], and so on. In the bilateral teleoperation system, the position and force signals are transmitted bidirectionally through the communication channel. The purpose of the control methods for the teleoperation system is to guarantee the stability of the system and implement satisfactory position tracking and force feedback performances [6].

However, some challenges often exist in controller design process of the teleoperation system. The time delay in communication channel is unavoidable, this would degrade the operating performance of the telerobotic system and even make the system instability. While, uncertainties of master/slave robots, operator, and environment dynamics, external disturbances, etc. can also make the system performance worse.

For decades, many control methods have been proposed to cope with these issues. The experimental methods [7], supervisory control [8], and software-based teleoperation method [9] are first used for the control of teleoperation systems [10]. Then the passivity-based approach is applied for control method design and stability investigation of the telerobotic system with time delays [11]. Since then, many passivity-based control methodologies have been proposed for position tracking control and bilateral control, such as scattering approach [12], [13] wave variables control [14], and improved wave variables control [15], [16]. Furthermore, some control strategies based on Lyapunov theory have been developed, including PD control [17], [18], sliding mode control [19], H_∞ control [20], output feedback control [21], and so on.

Adaptive control is a useful method to design the high performance control scheme for teleoperation system with poor structure of robot dynamic and operator/environment models. Li *et al.* [22] proposed a fuzzy adaptive control strategy for the teleoperation system, and multiple fuzzy logic systems are used to estimate multiple model uncertainties. In [23], the uncertainty parts in the telerobotic system are defined as a function, and the fuzzy logic systems are used to approximate this function. Yang *et al.* [24] proposed the prescribed performance control based on adaptive neural networks. In [25], the wave variable structure and radial basis function neural network (RBFNN) are combined for teleoperation control with time delays and model uncertainties. In [26], two different adaptive control schemes based on RBFNN are developed for position tracking in the teleoperation system. In [27], a projection mapping based on

Manuscript received November 13, 2019; revised July 8, 2020; accepted October 7, 2020. Date of publication November 10, 2020; date of current version February 17, 2022. This work was supported in part by the National Key Research and Development Program of China under Grant 2016YFB1001301; and in part by the National Natural Science Foundation of China under Grant 91648206 and Grant U1713210. This article was recommended by Associate Editor Z. Li. *(Corresponding author: Aiguo Song.)*

Haochen Zhang is with the State Key Laboratory of Bioelectronics, Jiangsu Key Laboratory of Remote Measurement and Control, School of Instrument Science and Engineering, Southeast University, Nanjing 210096, China, and also with the College of Electrical and Information Engineering, Lanzhou University of Technology, Lanzhou 730050, China (e-mail: lut_zhc@163.com).

Aiguo Song, Huijun Li, and Liqiang Fan are with the State Key Laboratory of Bioelectronics, Jiangsu Key Laboratory of Remote Measurement and Control, School of Instrument Science and Engineering, Southeast University, Nanjing 210096, China (e-mail: a.g.song@seu.edu.cn; lihuijun@seu.edu.cn; serpentfan@163.com).

Dapeng Chen is with the School of Automation, Nanjing University of Information Science and Technology, Nanjing 210044, China (e-mail: dpchen@nuist.edu.cn).

Color versions of one or more figures in this article are available at https://doi.org/10.1109/TSMC.2020.3032295.

Digital Object Identifier 10.1109/TSMC.2020.3032295

saturation is introduced, and the adaptive sliding mode control laws based on the RBF neural network are designed. In [28], a novel adaptive control scheme containing the RBFNN and the robust mechanism is presented. In [29], [30], and [38], the dynamic uncertain parts are, respectively, be linearly parameterized, and the adaptive controller and adaptive laws are designed. In addition, the principle of estimating the telerobotics uncertain model by using the fuzzy logic system and neural network is based on the universal approximation theorem. And the Lyapunov method is applied to design the controllers and adaptive laws.

However, the proposed adaptive methods above can only guarantee the stability and convergence of the system when the time goes to infinity [31]. In practical applications, it is expected that systems such as machinery and robot system can be able to achieve finite-time control performance [32]. Many finite-time control methods have been developed and applied to the system control process, which illustrates the advantages of finite-time control in terms of robustness, converge precision, and antidisturbance capabilities [31], [33]. In recent years, the adaptive finite-time control-based fuzzy logic system and neural network are studied and employ to deal with the problems of nonsmooth nonlinear systems [34], uncertain nonlinear models, input delay [35], unknown backlash-like [36], and odd rational numbers powers system [37]. These successful applications fully illustrate the effectiveness of the adaptive finite-time control method.

Therefore, the finite-time control approach [39]–[45] is also introduced into controller designing for providing the fast convergence, robustness, and high performance in teleoperation system. In [39] and [40], the novel fuzzy finite-time adaptive controllers are proposed for position synchronization performance in telerobotic system. The adaptive fuzzy method is employed to deal with the uncertainties in master and slave models. In [39], a new finite terminal sliding mode (TSM) is designed and the reaching time is given. In [40], the anti-windup compensator and switched filter system are introduced for finite-time controller design. Yang *et al.* [41] and Wang *et al.* [43], respectively, developed two finite-time controllers based on different nonsingular fast TSMs. Neural network is also introduced to estimate the model uncertainties, and the finite-time control scheme with error constrained [42], new integral TSM [44], and jittering free scheme [45] are, respectively, developed. It is noted that the time-varying delay is not considered in [41]–[43].

In real applications, the effective force tracking of the master and slave robots can make the system have better operational performance. Some research works have studied the force/torque tracking of the teleoperation system. In [46] and [47], the PD control and human torque compensation method are proposed for position tracking and force tracking. In [48], a feedback passivity controller is proposed, and the environment force measured by the force sensor is applied for force feedback. In [49], the torque error is introduced to construct the auxiliary function, and adaptive control scheme with position/torque tracking control are, respectively, developed. In [50]–[54], differential algorithms have been developed to estimate the environment force and external force, which are utilized for force compensating control. In [55], the SALS method is introduced to identify the parameters of dynamic and environment. In [56], the effect of time delay on model identification is considered, and a new control strategy for teleoperation control with large time delay is presented. It can be seen that the force/torque tracking control is mainly based on the measurement of the force/torque sensors and the force/environment estimation using the observer. However, using the observer to estimate the force/torque requires the accurate dynamic description of the robot. If there have the model uncertainties, it is obvious that this force/torque estimation method cannot be achieved.

Nevertheless, there still have some problems which are not considered in most of the above research works. First, many developed adaptive approaches mentioned above are implemented to provide position tracking performance, but force/torque tracking of master–slave robots is not considered (such as in [22]–[29] and [38]–[45]). Second, the position acceleration signals are introduced into the controller for control torque calculation (such as in work [22]–[24], [26]–[30], [40]–[42], [44], [45]). On the one hand, the differential of position error is applied for sliding mode surface and auxiliary variable function designing; on the other hand, the model uncertain part containing the mass inertia matrix is directly estimated by the adaptive method. In such cases, it can inevitably introduce the acceleration signals of master and slave robots. Finally, the finite-time control has not been used for position and force tracking control in existing research works.

In this article, we consider a teleoperation system with time-varying delay, parameterized uncertainties, and unknown spring-damper operator/environment models. The aim of this article is to achieve finite-time control of position and force tracking control in a teleoperation system with above conditions and challenges. That means we need to design a finite-time control structure which is different from traditional force tracking method. Furthermore, the proposed control scheme can also deal with the uncertain dynamics and time-varying delay of the teleoperation system, and has the position tracking capability as the existing work. Therefore, we construct a new auxiliary error system by using position and force tracking error, and design the finite-time adaptive control schemes. The RBFNN is applied to estimate the uncertain parts in the robot, human, and environment models. The main contributions of our work can be summarized as follows.

1) In this article, a new position-force hybrid tracking error subsystem is designed and a novel finite-time adaptive control scheme is y developed to achieve position and force tracking control in a teleoperation system. The asymmetric time-varying delays and unknown dynamics are considered in the system. Compared with the existing work with finite-time control [39]–[45], the position synchronization can be achieved and the force tracking of the master and slave robots can also be obtained. Compared with the position/force control method [23], [25], [27], [46]–[49], the finite-time control scheme can provide stronger robustness, faster and more precision convergence performance.

2) A new auxiliary variable function with finite-time structure is designed to avoid the use of the acceleration signals and smooth the velocity feedback signals. Different from existing work, the proposed auxiliary error function is composed of the hybrid error integral term, velocity feedback filter, and auxiliary velocity error, which can improve the position and force tracking performance and avoid use the acceleration and time delay information.

The remainder of this article is organized as follows. The preliminary descriptions are given in Section II. The proposed finite-time control scheme is presented in Section III. The stability and finite-time analysis are discussed in Section IV. Subsequently, the simulation and system experiment results and analysis are, respectively, illustrated in Sections V and VI. Finally, this work is concluded in Section VII.

II. System Modeling and Preliminary Description

In this section, we mainly describe the dynamic model of the teleoperation system, the problems addressed in our work, and some preliminary definitions and theorems.

A. Dynamic Description of Teleoperation System

The dynamic model of a typical master–slave teleoperation system with n degree of freedom (DOF) and revolute joints can be defined as follows:

$$\begin{cases} \boldsymbol{M}_m(\boldsymbol{q}_m)\ddot{\boldsymbol{q}}_m + \boldsymbol{C}_m(\dot{\boldsymbol{q}}_m, \boldsymbol{q}_m)\dot{\boldsymbol{q}}_m \\ \qquad +\boldsymbol{G}_m(\boldsymbol{q}_m) + \boldsymbol{B}_m = \boldsymbol{\tau}_m - \boldsymbol{F}_h \\ \boldsymbol{M}_s(\boldsymbol{q}_s)\ddot{\boldsymbol{q}}_s + \boldsymbol{C}_s(\dot{\boldsymbol{q}}_s\boldsymbol{q}_s)\dot{\boldsymbol{q}}_s \\ \qquad +\boldsymbol{G}_s(\boldsymbol{q}_s) + \boldsymbol{B}_s = \boldsymbol{\tau}_s - \boldsymbol{F}_e \end{cases} \tag{1}$$

where $\boldsymbol{q}_m, \boldsymbol{q}_s \in \mathcal{R}^n$, $\dot{\boldsymbol{q}}_m, \dot{\boldsymbol{q}}_s \in \mathcal{R}^n$, and $\ddot{\boldsymbol{q}}_m, \ddot{\boldsymbol{q}}_s \in \mathcal{R}^n$ are the joint position, joint velocity, and joint acceleration vectors of the master and slave robot, respectively. $\boldsymbol{M}_m(\boldsymbol{q}_m), \boldsymbol{M}_s(\boldsymbol{q}_s) \in \mathcal{R}^{n\times n}$ are the mass inertia matrices. $\boldsymbol{C}_m(\dot{\boldsymbol{q}}_m, \boldsymbol{q}_m), \boldsymbol{C}_s(\dot{\boldsymbol{q}}_s, \boldsymbol{q}_s) \in \mathcal{R}^{n\times n}$ are the centripetal and coriolis matrices. $\boldsymbol{G_m(q_m)}, \boldsymbol{G}_s(\boldsymbol{q}_s) \in \mathcal{R}^n$ are the gracitational vectors. $\boldsymbol{B}_m, \boldsymbol{B}_s \in \mathcal{R}^n$ are the friction vectors. $\boldsymbol{\tau}_m, \boldsymbol{\tau}_s \in \mathcal{R}^n$ are the control input torque vectors of master and slave manipulators. $\boldsymbol{F}_h \in \mathcal{R}^n$ is the human operator torque acting on the master manipulator. $\boldsymbol{F}_e \in \mathcal{R}^n$ is the environment torque applied to the slave manipulator. There are some well know properties on manipulator dynamic as shown below, which can be used for later theoretical analysis.

Property 1: The mass inertia matrices $\boldsymbol{M}_m(\boldsymbol{q}_m)$ and $\boldsymbol{M}_s(\boldsymbol{q}_s)$ are the symmetric, positive definite, and bounded matrices, which satisfy $\exists \chi_{j,min}, \chi_{j,max} > 0$, $0 < \chi_{j,min}\boldsymbol{I} \le \boldsymbol{M}_j \le \chi_{j,max}\boldsymbol{I}$, where $j = m, s$.

Property 2: $\dot{\boldsymbol{M}}_m - 2\boldsymbol{C}_m$ and $\dot{\boldsymbol{M}}_s - 2\boldsymbol{C}_s$ are the skew-symmetricmatrix, and for $j = m, s$, $\forall \boldsymbol{x} \in \mathcal{R}^n$ the equations $\boldsymbol{x}^{\mathrm{T}}(\dot{\boldsymbol{M}}_j - 2\boldsymbol{C}_j)\boldsymbol{x} = 0$ is always true.

In practical system, it is difficult to obtain exact dynamic parameters in (1). Thus, for $j = m, s$, the nominal models $\boldsymbol{M}_{jo}$, $\boldsymbol{C}_{jo}$, and $\boldsymbol{G}_{jo}$ are introduced to describe the know and nominal parts in teleoperation dynamic. The $\Delta\boldsymbol{M}_j$, $\Delta\boldsymbol{C}_j$, and $\Delta\boldsymbol{G}_j$ are used to represent the unknown parts, which we have

$$\begin{cases} \boldsymbol{M}_m = \boldsymbol{M}_{mo} + \Delta\boldsymbol{M}_m, \quad \boldsymbol{M}_s = \boldsymbol{M}_{so} + \Delta\boldsymbol{M}_s \\ \boldsymbol{C}_m = \boldsymbol{C}_{mo} + \Delta\boldsymbol{C}_m, \quad \boldsymbol{C}_s = \boldsymbol{C}_{so} + \Delta\boldsymbol{C}_s \\ \boldsymbol{G}_m = \boldsymbol{G}_{mo} + \Delta\boldsymbol{G}_m, \quad \boldsymbol{G}_s = \boldsymbol{G}_{so} + \Delta\boldsymbol{G}_s. \end{cases} \tag{2}$$

In this article, we consider the interaction torque of human operator and environment as the passive spring-damper model, which can be described as [46], [57]

$$\begin{aligned} \boldsymbol{F}_h &= \boldsymbol{f}_h + \boldsymbol{D}_h\dot{\boldsymbol{q}}_m + \boldsymbol{S}_h\boldsymbol{q}_m \\ \boldsymbol{F}_e &= \boldsymbol{f}_e + \boldsymbol{D}_e\dot{\boldsymbol{q}}_s + \boldsymbol{S}_e\boldsymbol{q}_s \end{aligned} \tag{3}$$

where $\boldsymbol{D}_h, \boldsymbol{D}_e \in \mathcal{R}^{n\times n}$ denote the damping matrices of the operator and environment. $\boldsymbol{S}_h, \boldsymbol{S}_e \in \mathcal{R}^{n\times n}$ express the spring matrices of the operator and environment. $\boldsymbol{D}_h$, $\boldsymbol{D}_e$, $\boldsymbol{S}_h$, and $\boldsymbol{S}_e$ are all positive definite and diagonal constant matrices. $\boldsymbol{f}_h$ and $\boldsymbol{f}_e$ are the extra operator and environment torque, and they follow the assumption below.

Assumption 1: The external operator torque $\boldsymbol{f}_h$ and external environment torque $\boldsymbol{f}_e$ are all bounded.

We define $d_m(t)$ as the varying communication time delay from the master side to the slave side, and $d_s(t)$ is the time-varying delay from the slave robot to master robot. There has an assumption about time delays $d_m(t)$ and $d_s(t)$ as

Assumption 2: For $j = m, s$, the time-varying delay $d_j(t) \ge 0$ and change rate $\dot{d}_j(t)$ are all bounded. In addition, $0 \le d_j(t) \le \bar{d}_j$, $|\dot{d}_j(t)| \le D_j$.

B. Problem Formulation and Control Object

We define the joint position tracking errors $\boldsymbol{e}_m$ and $\boldsymbol{e}_s$ as

$$\begin{aligned} \boldsymbol{e}_m(t) &= \boldsymbol{q}_m(t) - \boldsymbol{q}_s(t - d_s) \\ \boldsymbol{e}_s(t) &= \boldsymbol{q}_s(t) - \boldsymbol{q}_m(t - d_m). \end{aligned} \tag{4}$$

Similarly, we define force tracking errors $\boldsymbol{\Delta F}_m$ and $\boldsymbol{\Delta F}_s$ as

$$\begin{aligned} \boldsymbol{\Delta F}_m(t) &= \boldsymbol{F}_h(t) - \boldsymbol{F}_e(t - d_s) \\ \boldsymbol{\Delta F}_s(t) &= \boldsymbol{F}_e(t) - \boldsymbol{F}_h(t - d_m). \end{aligned} \tag{5}$$

Therefore, considering the teleoperation system dynamic (1) with uncertain model parameters, human operator and environment models (3), and varying communication time delays, the appropriate control laws $\boldsymbol{\tau}_m$ and $\boldsymbol{\tau}_s$ need to be designed to accomplish the following control objects.

1) *Stability Performance:* The closed-loop teleoperation system needs to be stable under time-varying delays, dynamic uncertainties, and bounded external operator torque disturbances.
2) *Position Tracking Performance:* Make the slave robot can track the joint position of the master robot. At the same time, the master robot can also track the joint position of the slave robot. It indicates that the position tracking error $\boldsymbol{e}_m$ and $\boldsymbol{e}_s$ can reach into a small neighbor.
3) *Force Feedback Tracking Performance:* Ensure the torque tracking error $\Delta\boldsymbol{F}_m$ and $\Delta\boldsymbol{F}_s$ can converge into a small neighbor of 0, which can make the human operator feel the actual torque from the environment. Although mentioned in 2), the master-to-slave position tracking can obtain the certain force feedback, but the intensity of the force feedback is uncertain and may be large or small. Therefore, it is needed to exert sufficient force feedback consistent with environment torque.

C. RBF Neural Network

In our work, the adaptive control method with the RBFNN is employed to deal with the dynamic uncertainties. The RBFNN can estimate and approximate an uncertain continuous function $F(\boldsymbol{x}): \mathcal{R}^a \to \mathcal{R}^b$ as

$$F(\boldsymbol{x}) = \boldsymbol{W}^{\mathrm{T}}\boldsymbol{\varphi}(\boldsymbol{x}) + \boldsymbol{\epsilon} \tag{6}$$

where $\boldsymbol{W} \in \mathcal{R}^{c\times a}$ is the weight matrix, c is the node number of neural network. $\boldsymbol{\varphi}(\boldsymbol{x}) \in \mathcal{R}^c$ is the Gaussian basis function vector. $\boldsymbol{\epsilon}$ is the bounded approximation error [58]. Gaussian basis function vector $\boldsymbol{\varphi}(\boldsymbol{x})$ can be calculated by

$$\boldsymbol{\varphi}(\boldsymbol{x}) = e^{-\frac{(\boldsymbol{x}-\boldsymbol{d}_i)^{\mathrm{T}}(\boldsymbol{x}-\boldsymbol{d}_i)}{2f^2}}, i = 1, 2, \ldots, c \tag{7}$$

where $\boldsymbol{d}_i \in \mathcal{R}^a$ is the center vector of Gaussian function, f is the width of the Gaussian function.

D. Preliminary Lemmas

There are two lemmas used for system stability analysis and proof.

Lemma 1 [59]: For any $a_1, a_2, \ldots, a_n \in \mathcal{R}$ and $0 < b < 1$, there has the following inequality holds:

$$(|a_1| + |a_2| + \cdots + |a_n|)^b \le |a_1|^b + |a_2|^b + \cdots + |a_n|^b.$$

Lemma 2 [60]: Considering the system dynamics as $\dot{\boldsymbol{x}} = \boldsymbol{f}(\boldsymbol{x})$, $\boldsymbol{x} \in \mathcal{R}$, and $\boldsymbol{x}(0) = \boldsymbol{x}_0$. The system is finite-time stable and can converge to a neighborhood in finite-time T_s, if there is a positive differentiable scalar function $V(\boldsymbol{x})$ and makes the following inequality establishes:

$$\dot{V}(\boldsymbol{x}) \le -\alpha V(\boldsymbol{x}) - \beta V^{\sigma}(\boldsymbol{x})$$

where $\alpha, \beta > 0$, $0 < \sigma < 1$. The setting time T_{set} can be described as

$$T_{set} \le \frac{1}{\alpha(1-\sigma)} \ln \frac{\alpha V^{1-\sigma}(\boldsymbol{x}_0) + \beta}{\beta}.$$

III. Control Design and Analysis

This section elaborates on the design of the proposed auxiliary error system, the auxiliary variable, and the finite-time controller. First, a novel auxiliary error system is constructed based on the position tracking error. Second, the new master and slave integral auxiliary variables are designed for the controllers design based on the auxiliary error system and angular velocity feedback filter. Third, the RBFNN is used to estimate and compensate for the uncertainty of dynamics. Finally, the finite-time control laws and adaptive laws for the master and slave robots are given.

A. Auxiliary Error System and Integral Auxiliary Variables Design

Define the torque error filters $\boldsymbol{\alpha}_m$ and $\boldsymbol{\alpha}_s$ as

$$\begin{aligned} \dot{\boldsymbol{\alpha}}_m &= -\boldsymbol{L}_{m1}\boldsymbol{\alpha}_m + \boldsymbol{L}_{m1}\boldsymbol{\Delta F}_m \\ \dot{\boldsymbol{\alpha}}_s &= -\boldsymbol{L}_{s1}\boldsymbol{\alpha}_s + \boldsymbol{L}_{s1}\boldsymbol{\Delta F}_s \end{aligned} \tag{8}$$

where $\boldsymbol{L}_{m1}$ and $\boldsymbol{L}_{s1}$ are positive-definite symmetric matrices.

We combine the position tracking errors $\boldsymbol{e}_m$, $\boldsymbol{e}_s$ and the torque error filters $\boldsymbol{\alpha}_m$, $\boldsymbol{\alpha}_s$ to define and build the novel hybrid auxiliary error systems $\boldsymbol{r}_m$ and $\boldsymbol{r}_s$ as

$$\begin{aligned} \boldsymbol{r}_m &= \boldsymbol{\eta}_{m1}\boldsymbol{e}_m + \boldsymbol{\eta}_{m2}\boldsymbol{\alpha}_m \\ \boldsymbol{r}_s &= \boldsymbol{\eta}_{s1}\boldsymbol{e}_s + \boldsymbol{\eta}_{s2}\boldsymbol{\alpha}_s \end{aligned} \tag{9}$$

where $\boldsymbol{\eta}_{m1}$, $\boldsymbol{\eta}_{m2}$, $\boldsymbol{\eta}_{s1}$, and $\boldsymbol{\eta}_{s2}$ are the weight values of position and torque tracking errors, they are all positive constants. Then the auxiliary variables and controllers can be designed based on $\boldsymbol{r}_m$ and $\boldsymbol{r}_s$.

The differential of $\boldsymbol{r}_m$ and $\boldsymbol{r}_s$ can be expressed as

$$\begin{aligned} \dot{\boldsymbol{r}}_m &= \boldsymbol{\eta}_{m1}\dot{\boldsymbol{e}}_m + \boldsymbol{\eta}_{m2}\dot{\boldsymbol{\alpha}}_m \\ \dot{\boldsymbol{r}}_s &= \boldsymbol{\eta}_{s1}\dot{\boldsymbol{e}}_s + \boldsymbol{\eta}_{s2}\dot{\boldsymbol{\alpha}}_s. \end{aligned} \tag{10}$$

Remark 1: The auxiliary error system consists of the position tracking error and force tracking error. The values of $\boldsymbol{\eta}_{m1}$, $\boldsymbol{\eta}_{m2}$, $\boldsymbol{\eta}_{s1}$, and $\boldsymbol{\eta}_{s2}$ can be used to adjust the weight of position and force tracking errors in $\boldsymbol{r}_m$ and $\boldsymbol{r}_s$. Therefore, by introducing the auxiliary error system, the problem of position and force tracking is transformed into the problem of making the error system $\boldsymbol{r}_m$ and $\boldsymbol{r}_s$ stable. On the other hand, we need to differential the auxiliary errors $\boldsymbol{r}_m$ and $\boldsymbol{r}_s$ to get the expression in (10). If the force tracking errors $\boldsymbol{\Delta F}_m$ and $\boldsymbol{\Delta F}_s$ are directly used to design the $\boldsymbol{r}_m$ and $\boldsymbol{r}_s$ instead of the output of force tracking error filter $\boldsymbol{\alpha}_m$ and $\boldsymbol{\alpha}_s$, it is obvious that the $\boldsymbol{\Delta F}_m$ and $\boldsymbol{\Delta F}_s$ need to be differentiated when the differential of $\boldsymbol{r}_m$ and $\boldsymbol{r}_s$ are obtained. Therefore, it is unnecessary to introduce the additional differential signals of force tracking errors $\boldsymbol{\Delta \dot{F}}_m$ and $\boldsymbol{\Delta \dot{F}}_s$ based on force tracking error filters $\boldsymbol{\alpha}_m$ and $\boldsymbol{\alpha}_s$. In the following auxiliary variable design, we also design the velocity feedback filter to avoid the use of accelerating signals.

The derivative of position tracking errors $\dot{\boldsymbol{e}}_m$ and $\dot{\boldsymbol{e}}_s$ are obtained as

$$\begin{aligned} \dot{\boldsymbol{e}}_m &= \dot{\boldsymbol{q}}_m(t) - \dot{\boldsymbol{q}}_s(t-d_s)(1-\dot{d}_s) \\ \dot{\boldsymbol{e}}_s &= \dot{\boldsymbol{q}}_s(t) - \dot{\boldsymbol{q}}_m(t-d_m)(1-\dot{d}_m). \end{aligned} \tag{11}$$

Obviously, the change rates $\dot{d}_m$ and $\dot{d}_s$ of communication time delay, which is difficult to be obtained in the actual system, are introduced into the angular velocity errors. We define a new form of joint velocity errors $\boldsymbol{e}_{mv}$ and $\boldsymbol{e}_{sv}$ to facilitate and simplify the $\dot{\boldsymbol{e}}_m$ and $\dot{\boldsymbol{e}}_s$ as

$$\begin{aligned} \boldsymbol{e}_{mv} &= \dot{\boldsymbol{q}}_m(t) - \dot{\boldsymbol{q}}_s(t-d_s) \\ \boldsymbol{e}_{sv} &= \dot{\boldsymbol{q}}_s(t) - \dot{\boldsymbol{q}}_m(t-d_m). \end{aligned} \tag{12}$$

Then the $\dot{\boldsymbol{e}}_m$, $\dot{\boldsymbol{e}}_s$, $\dot{\boldsymbol{r}}_m$, and $\dot{\boldsymbol{r}}_s$ can be written as

$$\begin{aligned} \dot{\boldsymbol{e}}_m &= \boldsymbol{e}_{mv} + \dot{\boldsymbol{q}}_s(t-d_s)\dot{d}_s \\ \dot{\boldsymbol{e}}_s &= \boldsymbol{e}_{sv} + \dot{\boldsymbol{q}}_m(t-d_m)\dot{d}_m \\ \dot{\boldsymbol{r}}_m &= \boldsymbol{\eta}_{m1}\boldsymbol{e}_{mv} + \boldsymbol{\eta}_{m2}\dot{\boldsymbol{\alpha}}_m + \boldsymbol{\eta}_{m1}\dot{\boldsymbol{q}}_s(t-d_s)\dot{d}_s \\ \dot{\boldsymbol{r}}_s &= \boldsymbol{\eta}_{s1}\boldsymbol{e}_{sv} + \boldsymbol{\eta}_{s2}\dot{\boldsymbol{\alpha}}_s + \boldsymbol{\eta}_{s1}\dot{\boldsymbol{q}}_m(t-d_m)\dot{d}_m. \end{aligned} \tag{13}$$

We propose and design the novel integral auxiliary variables $\boldsymbol{s}_m$ and $\boldsymbol{s}_s$ by coupling the auxiliary error system $\boldsymbol{r}_m$ and $\boldsymbol{r}_s$, the joint velocity feedback filter $\boldsymbol{v}_m$ and $\boldsymbol{v}_s$, and finite-time-integral terms of $\boldsymbol{r}_m$ and $\boldsymbol{r}_s$. Then we can design the suitable

finite-time controller for the teleoperation system based on $\boldsymbol{s}_m$ and $\boldsymbol{s}_s$. The $\boldsymbol{s}_m$ and $\boldsymbol{s}_s$ are defined as

$$\begin{aligned}\boldsymbol{s}_m &= \boldsymbol{E}_{mv} + \boldsymbol{\vartheta}_m \\ \boldsymbol{s}_s &= \boldsymbol{E}_{sv} + \boldsymbol{\vartheta}_s\end{aligned} \tag{14}$$

where $\boldsymbol{E}_{mv}$ and $\boldsymbol{E}_{sv}$ are the auxiliary angular velocity error functions including the joint velocity feedback filters, which can be defined as

$$\begin{aligned}\boldsymbol{E}_{mv} &= \dot{\boldsymbol{q}}_m - \boldsymbol{v}_m \\ \boldsymbol{E}_{sv} &= \dot{\boldsymbol{q}}_s - \boldsymbol{v}_s\end{aligned} \tag{15}$$

where $\boldsymbol{v}_m$ and $\boldsymbol{v}_s$ are the output of the joint velocity feedback filter from the slave side and the master side, respectively, which can be described as

$$\begin{aligned}\dot{\boldsymbol{v}}_m &= -\boldsymbol{L}_{m2}\boldsymbol{v}_m + \boldsymbol{L}_{m2}\dot{\boldsymbol{q}}_s(t-d_s) \\ \dot{\boldsymbol{v}}_s &= -\boldsymbol{L}_{s2}\boldsymbol{v}_s + \boldsymbol{L}_{s2}\dot{\boldsymbol{q}}_m(t-d_m).\end{aligned} \tag{16}$$

Remark 2: Similar to the force tracking error filter $\boldsymbol{\alpha}_m, \boldsymbol{\alpha}_s$ and the description in *Remark 1*, we also devised the velocity feedback filters $\boldsymbol{v}_m, \boldsymbol{v}_s$ and novel auxiliary velocity error functions $\boldsymbol{E}_{mv}, \boldsymbol{E}_{sv}$ to avoid the use of acceleration signals. Compared with some existing research work, similar auxiliary variables are typically designed based on velocity errors as $\boldsymbol{s}_j = \dot{\boldsymbol{e}}_j + \lambda_j \boldsymbol{\beta}_j(\boldsymbol{e}_j)$, where $j = m, s$, and $\boldsymbol{\beta}_j(\boldsymbol{e}_j)$ is the function of $\boldsymbol{e}_j$. For this form of auxiliary variable, the acceleration signal is inevitably used for the designing of controllers. However, in practice, we do not want to introduce the acceleration signal to calculate the control law, as it may contain more noise. Therefore, the proposed and designed velocity feedback filter and auxiliary function in our work can avoid the acceleration signal being used.

The finite-time-integral functions $\boldsymbol{\vartheta}_m$ and $\boldsymbol{\vartheta}_s$ in $\boldsymbol{s}_m$ and $\boldsymbol{s}_s$ are, respectively, defined as

$$\begin{aligned}\boldsymbol{\vartheta}_m &= \boldsymbol{\lambda}_{m1}\mathrm{sig}(\boldsymbol{r}_m)^{\sigma_{m1}} + \boldsymbol{\lambda}_{m2}\int_0^t \mathrm{sig}(\boldsymbol{r}_m)^{\sigma_{m2}}\,\mathrm{d}\tau \\ \boldsymbol{\vartheta}_s &= \boldsymbol{\lambda}_{s1}\mathrm{sig}(\boldsymbol{r}_s)^{\sigma_{s1}} + \boldsymbol{\lambda}_{s2}\int_0^t \mathrm{sig}(\boldsymbol{r}_s)^{\sigma_{s2}}\,\mathrm{d}\tau\end{aligned} \tag{17}$$

where $\boldsymbol{\lambda}_{m1}$, $\boldsymbol{\lambda}_{m2}$, $\boldsymbol{\lambda}_{s1}$, and $\boldsymbol{\lambda}_{s2}$ are the weight coefficients, and they are all positive diagonal matrices. $1 < \sigma_{m1}, \sigma_{s1} < 2$ and $0 < \sigma_{m2}, \sigma_{s2} < 1$. For any vector $\boldsymbol{x} \in \mathcal{R}^n$, $\boldsymbol{x} = [x_1, x_2, \ldots, x_n]$, $\mathrm{sig}(\boldsymbol{x}) = [|x_1|\mathrm{sign}(x_1), |x_2|\mathrm{sign}(x_2), \ldots, |x_n|\mathrm{sign}(x_n)]$.When $r > 0$, $\mathrm{sig}(\boldsymbol{x})^r = [|x_1|^r\mathrm{sign}(x_1), |x_2|^r\mathrm{sign}(x_2), \ldots, |x_n|^r\mathrm{sign}(x_n)]$.

Then we can have the differential of $\boldsymbol{s}_m$ and $\boldsymbol{s}_s$ as

$$\begin{aligned}\dot{\boldsymbol{s}}_m &= \dot{\boldsymbol{E}}_{mv} + \dot{\boldsymbol{\vartheta}}_m \\ \dot{\boldsymbol{s}}_s &= \dot{\boldsymbol{E}}_{sv} + \dot{\boldsymbol{\vartheta}}_s\end{aligned} \tag{18}$$

where $\dot{\boldsymbol{E}}_{mv}$ and $\dot{\boldsymbol{E}}_{sv}$ are

$$\begin{aligned}\dot{\boldsymbol{E}}_{mv} &= \ddot{\boldsymbol{q}}_m - \dot{\boldsymbol{v}}_m \\ \dot{\boldsymbol{E}}_{sv} &= \ddot{\boldsymbol{q}}_s - \dot{\boldsymbol{v}}_s.\end{aligned} \tag{19}$$

$\dot{\boldsymbol{\vartheta}}_m$ and $\dot{\boldsymbol{\vartheta}}_s$ are

$$\begin{aligned}\dot{\boldsymbol{\vartheta}}_m &= \sigma_{m1}\boldsymbol{\lambda}_{m1}\mathrm{diag}(|\boldsymbol{r}_m|)^{\sigma_{m1}-1}\dot{\boldsymbol{r}}_m + \boldsymbol{\lambda}_{m2}\mathrm{sig}(\boldsymbol{r}_m)^{\sigma_{m2}} \\ \dot{\boldsymbol{\vartheta}}_s &= \sigma_{s1}\boldsymbol{\lambda}_{s1}\mathrm{diag}(|\boldsymbol{r}_s|)^{\sigma_{s1}-1}\dot{\boldsymbol{r}}_s + \boldsymbol{\lambda}_{s2}\mathrm{sig}(\boldsymbol{r}_s)^{\sigma_{s2}}.\end{aligned} \tag{20}$$

Next, the RBFNN is used to approximate and estimate the uncertain parts of the teleoperation dynamics.

B. Approximation of Dynamic Uncertainties

Based on the system dynamic description (1), (3), and (18)–(20) we can obtain $\boldsymbol{M}_j\dot{\boldsymbol{s}}_j$ as

$$\begin{aligned}\boldsymbol{M}_j\dot{\boldsymbol{s}}_j &= \boldsymbol{M}_j\ddot{\boldsymbol{q}}_j + \boldsymbol{M}_j\Big[-\dot{\boldsymbol{v}}_j + \sigma_{j1}\boldsymbol{\lambda}_{j1}\mathrm{diag}(|\boldsymbol{r}_j|)^{\sigma_{j1}-1}\dot{\boldsymbol{r}}_j \\ &\quad + \boldsymbol{\lambda}_{j2}\mathrm{sig}(\boldsymbol{r}_j)^{\sigma_{j2}}\Big] \\ &= \boldsymbol{M}_j\ddot{\boldsymbol{q}}_j + \boldsymbol{M}_j\Big[-\dot{\boldsymbol{v}}_j + \sigma_{j1}\boldsymbol{\lambda}_{j1}\mathrm{diag}(|\boldsymbol{r}_j|)^{\sigma_{j1}-1} \\ &\quad \big(\boldsymbol{\eta}_{j1}\boldsymbol{e}_{jv} + \boldsymbol{\eta}_{j2}\dot{\boldsymbol{\alpha}}_j\big) + \boldsymbol{\lambda}_{j2}\mathrm{sig}(\boldsymbol{r}_j)^{\sigma_{j2}}\Big] \\ &\quad + \sigma_{j1}\boldsymbol{M}_j\boldsymbol{\lambda}_{j1}\mathrm{diag}(|\boldsymbol{r}_j|)^{\sigma_{j1}-1}\boldsymbol{\eta}_{j1}\dot{\boldsymbol{q}}_{j'}(t-d_{j'})\dot{d}_{j'}\end{aligned} \tag{21}$$

where for $j = m, s$ and $j' = s, m$.

We define $\boldsymbol{\mu}_{j1}$, $\boldsymbol{\mu}_{j2}$, and $\boldsymbol{\mu}_{j3}$ to simplify the follow-up describtion as

$$\begin{aligned}\boldsymbol{\mu}_{j1} &= -\dot{\boldsymbol{v}}_j + \sigma_{j1}\boldsymbol{\lambda}_{j1}\mathrm{diag}(|\boldsymbol{r}_j|)^{\sigma_{j1}-1}\big(\boldsymbol{\eta}_{j1}\boldsymbol{e}_{jv} \\ &\quad + \boldsymbol{\eta}_{j2}\dot{\boldsymbol{\alpha}}_j\big) + \boldsymbol{\lambda}_{j2}\mathrm{sig}(\boldsymbol{r}_j)^{\sigma_{j2}} \\ \boldsymbol{\mu}_{j2} &= \sigma_{j1}\boldsymbol{\lambda}_{j1}\mathrm{diag}(|\boldsymbol{r}_j|)^{\sigma_{j1}-1}\boldsymbol{\eta}_{j1}\dot{\boldsymbol{q}}_{j'}(t-d_{j'}), \\ \boldsymbol{\mu}_{j3} &= \boldsymbol{s}_j - \dot{\boldsymbol{q}}_j.\end{aligned} \tag{22}$$

Then based on the dynamics and uncertain description of teleoperation system in (1)–(3), the $\boldsymbol{M}_j\dot{\boldsymbol{s}}_j$ can be rewritten as

$$\begin{aligned}\boldsymbol{M}_j\dot{\boldsymbol{s}}_j &= \boldsymbol{\tau}_j - \boldsymbol{f}_{he,j} + \boldsymbol{M}_{jo}\boldsymbol{\mu}_{j1} + \boldsymbol{M}_{jo}\boldsymbol{\mu}_{j2}\dot{d}_{j'} + \boldsymbol{C}_{jo}\boldsymbol{\mu}_{j3} \\ &\quad - \boldsymbol{G}_{jo} + \Delta\boldsymbol{M}_j\boldsymbol{\mu}_{j1} + \Delta\boldsymbol{M}_j\boldsymbol{\mu}_{j2}\dot{d}_{j'} + \Delta\boldsymbol{C}_j\boldsymbol{\mu}_{j3} \\ &\quad - \Delta\boldsymbol{G}_j - \boldsymbol{B}_j - \boldsymbol{D}_{he,j}\dot{\boldsymbol{q}}_j - \boldsymbol{S}_{he,j}\boldsymbol{q}_j - \boldsymbol{C}_j\boldsymbol{s}_j \\ &= \boldsymbol{\tau}_j - \boldsymbol{f}_{he,j} + \boldsymbol{M}_{jo}\boldsymbol{\mu}_{j1} + \boldsymbol{M}_{jo}\boldsymbol{\mu}_{j2}\dot{d}_{j'} + \boldsymbol{C}_{jo}\boldsymbol{\mu}_{j3} \\ &\quad - \boldsymbol{G}_{jo} + \boldsymbol{P}_j - \boldsymbol{C}_j\boldsymbol{s}_j\end{aligned} \tag{23}$$

where for $j = m$, $\boldsymbol{f}_{he,j} = \boldsymbol{f}_h$, $\boldsymbol{D}_{he,j} = \boldsymbol{D}_h$, and $\boldsymbol{S}_{he,j} = \boldsymbol{S}_h$. For $j = s$, $\boldsymbol{f}_{he,j} = \boldsymbol{f}_e$, $\boldsymbol{D}_{he,j} = \boldsymbol{D}_e$, and $\boldsymbol{S}_{he,j} = \boldsymbol{S}_e$. Then we define the uncertain part of teleoperation system $\boldsymbol{P}_j = \Delta\boldsymbol{M}_j\boldsymbol{\mu}_{j1} + \Delta\boldsymbol{M}_j\boldsymbol{\mu}_{j2}\dot{d}_{j'} + \Delta\boldsymbol{C}_j\boldsymbol{\mu}_{j3} - \Delta\boldsymbol{G}_j - \boldsymbol{B}_j - \boldsymbol{D}_{he,j}\dot{\boldsymbol{q}}_j - \boldsymbol{S}_{he,j}\boldsymbol{q}_j$. It should be noted that the change rate $\dot{d}_{j'}$ is introduced into the uncertain part. In the system, the change rate of time delay may be unknown, so we define $\Delta\boldsymbol{M}_j\dot{d}_{j'}$ as an uncertain part in $\boldsymbol{P}_j$, and use RBFNN to estimate it. Therefore, the input of RBFNN is set as $\boldsymbol{Z}_j = [\boldsymbol{\mu}_{j1}^{\mathrm{T}}, \boldsymbol{\mu}_{j2}^{\mathrm{T}}, \boldsymbol{\mu}_{j3}^{\mathrm{T}}, \boldsymbol{q}_j^{\mathrm{T}}, \dot{\boldsymbol{q}}_j^{\mathrm{T}}]$. Then, the uncertain function $\boldsymbol{P}_j$ can be described as

$$\boldsymbol{P}_j = \boldsymbol{\theta}_j^{\mathrm{T}}\boldsymbol{Y}_j(\boldsymbol{Z}_j) + \boldsymbol{\epsilon}_j \tag{24}$$

where $\boldsymbol{\theta}_j \in \mathcal{R}^{l\times n}$ is the ideal approximation parameter matrix; l is the number of hidden layer nodes in RBFNN; $\boldsymbol{\epsilon}_j \in \mathcal{R}^{n\times 1}$ is the approximation error and is bunded; $\boldsymbol{Y}(\boldsymbol{Z}_j) = [y_{j1}(\boldsymbol{Z}_j), y_{j2}(\boldsymbol{Z}_j). \ldots, y_{jl}(\boldsymbol{Z}_j)] \in \mathcal{R}^{l\times 1}$ is the Gaussian basis function vector of RBFNN, and can be calculated as

$$y_{ji}(\boldsymbol{Z}_j) = e^{-\frac{(\boldsymbol{Z}_j - \boldsymbol{c}_i)^{\mathrm{T}}(\boldsymbol{Z}_j - \boldsymbol{c}_i)}{2b_j^2}}, i = 1, 2, \ldots, l. \tag{25}$$

$\boldsymbol{c}_i \in \mathcal{R}^{1\times 5n}$ is the center vector of Gaussian function of the ith hidden layer node; b_j is the width of Gaussian function.

Remark 3: The approximation error $\boldsymbol{\epsilon}_j$ is bounded for $j = m, s$, when using the RBFNN to estimate the dynamic uncertain part. With the assumption of bounded $\boldsymbol{f}_{he,j}$, it can

be drawn that $\|\boldsymbol{f}_{he,j}+\boldsymbol{\epsilon}_j\|$ is bounded, and there exists a positive constant ω_j such that $\|\boldsymbol{f}_{he,j}+\boldsymbol{\epsilon}_j\|^2 \le \omega_j$.

Remark 4: It is obvious that $\boldsymbol{P}_m$ and $\boldsymbol{P}_s$ contain the uncertain parts of the master–slave robot dynamic, the human operator model and the environment model. In our work, we consider the Lyapunov candidate function $V_1 = 1/2\boldsymbol{s}_m^{\mathrm{T}}\boldsymbol{M}_m\boldsymbol{s}_m + 1/2\boldsymbol{s}_s^{\mathrm{T}}\boldsymbol{M}_s\boldsymbol{s}_s$, and described the $\boldsymbol{M}_m\dot{\boldsymbol{s}}_m$ and $\boldsymbol{M}_s\dot{\boldsymbol{s}}_s$ which are the main items of V_1 differential result. In most of the existing work, the model uncertainty description in (2) is directly brought into the dynamic models (1) to obtain a new form of dynamics as

$$\boldsymbol{M}_{jo}\ddot{\boldsymbol{q}}_j + \boldsymbol{C}_{jo}\dot{\boldsymbol{q}}_j + \boldsymbol{G}_{jo} = \tau_j - \underbrace{\begin{array}{l}\Delta\boldsymbol{M}_j\ddot{\boldsymbol{q}}_j - \Delta\boldsymbol{C}_j\dot{\boldsymbol{q}}_j - \Delta\boldsymbol{G}_{jo} \\ -\boldsymbol{f}_{he,j} - \boldsymbol{D}_{he,j}\dot{\boldsymbol{q}}_j - \boldsymbol{S}_{he,j}\boldsymbol{q}_j\end{array}}_{\text{uncertain part}}.$$

When utilizing the RBFNN to estimate the uncertainty parts described above, the acceleration signals also need to be used. In our work, It is evident that there is no need for the acceleration signal when applying the RBFNN to approximate the $\boldsymbol{P}_m$ and $\boldsymbol{P}_s$.

C. Controller Design

The block diagram of the proposed control system is shown in Fig. 1. The proposed controllers are composed of the nominal model controller, RBFNN-adaptive controller, and finite-time controller, which are given as follows. The torque error filters $\boldsymbol{\alpha}_m, \boldsymbol{\alpha}_s$, velocity feedback filters $\boldsymbol{v}_m, \boldsymbol{v}_s$, auxiliary error systems $\boldsymbol{r}_m, \boldsymbol{r}_s$, and auxiliary variable $\boldsymbol{s}_m, \boldsymbol{s}_s$ have been defined above. When $j = m, s$, there has $j' = s, m$, the proposed control law $\boldsymbol{\tau}_j$ can be designed as

$$\begin{aligned}\boldsymbol{\tau}_j = &-\boldsymbol{M}_{jo}\boldsymbol{\mu}_{j1} - \boldsymbol{C}_{jo}\boldsymbol{\mu}_{j3} + \boldsymbol{G}_{jo} \\ &- \hat{\boldsymbol{\theta}}_j^{\mathrm{T}}\boldsymbol{Y}_j(\boldsymbol{Z}_j) - \frac{\hat{D}_{j'}\|\boldsymbol{M}_{jo}\boldsymbol{\mu}_{j2}\|^2}{2a_{j1}^2}\boldsymbol{s}_j - \frac{\hat{\omega}_j}{2a_{j2}^2}\boldsymbol{s}_j \\ &- \boldsymbol{K}_{j1}\boldsymbol{s}_j - \boldsymbol{K}_{j2}\mathrm{sig}(\boldsymbol{s}_j)^{\sigma}\end{aligned} \tag{26}$$

where $\boldsymbol{K}_{j1}, \boldsymbol{K}_{j2} \in \mathcal{R}^{n\times n}$ are the diagonal positive-definite matrices. $a_{j1}, a_{j2} \in \mathcal{R}$ are the positive constants.

The adaptive laws can be designed as

$$\begin{aligned}\dot{\hat{\boldsymbol{\theta}}}_j &= \boldsymbol{\Gamma}_{j1}\boldsymbol{Y}_j(\boldsymbol{Z}_j)\boldsymbol{s}_j^{\mathrm{T}} - \hat{\boldsymbol{\theta}}_j \\ \dot{\hat{D}}_{j'} &= \frac{\Gamma_{j2}}{2a_{j1}^2}\boldsymbol{s}_j^{\mathrm{T}}\boldsymbol{s}_j\|\boldsymbol{M}_{jo}\boldsymbol{\mu}_{j2}\|^2 - \hat{D}_{j'} \\ \dot{\hat{\omega}}_j &= \frac{\Gamma_{j3}}{2a_{j2}^2}\boldsymbol{s}_j^{\mathrm{T}}\boldsymbol{s}_j - \hat{\omega}_j\end{aligned} \tag{27}$$

where $\boldsymbol{\Gamma}_{j1} \in \mathcal{R}^{n\times n}$ is the diagonal positive-definite matrix. $\Gamma_{j2}, \Gamma_{j3} \in \mathcal{R}$ are the positive constants.

Finally, the closed-loop teleoperation system based on our proposed control method is consisted of the dynamics (1)–(3), position and force tracking errors (4), (5), force error filter (8), combined error system (9), auxiliary variable (14), velocity feedback filter (16), control law (26), and adaptive laws (27).

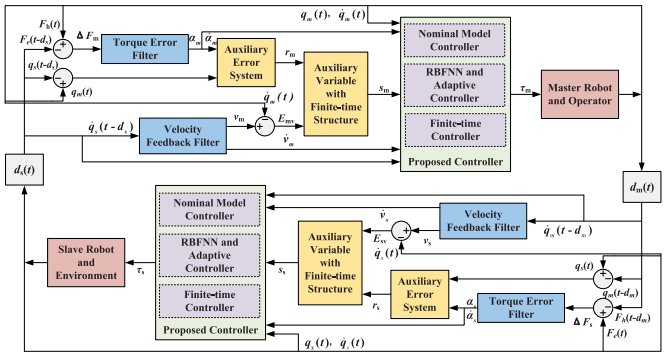

Fig. 1. Proposed control structure for the teleoperaton system.

IV. Stability Analysis

Theorem 1: Having the combined auxiliary error system in (9), force tracking error filter (8), velocity feedback filter in (16), and auxiliary variable (14), considering the teleoperation system (1) with human operator and environment model (2), dynamic uncertain (3), adaptive finite-time control law in (26), and adaptive laws in (27), the closed-loop system is asymptotically stable and having the finite-time performance, if the control parameters $\boldsymbol{K}_{j1}, \boldsymbol{K}_{j2}, \boldsymbol{\Gamma}_{j1}$ are all positive-definite diagonal matrices, $a_{j1}, a_{j2}, \Gamma_{j2}, \Gamma_{j3}$ are all positive constants, and $0 < \sigma < 1$.

Then we will give the proof process of this theorem.

Proof: We define the Lyapunov–Krasovskii functuin V as

$$V = V_1 + V_2 + V_3 \tag{28}$$

where for $j = m, s$, $j' = s, m$

$$\begin{aligned}V_1 &= \sum_{j=m,s}\frac{1}{2}\boldsymbol{s}_j^{\mathrm{T}}\boldsymbol{M}_j\boldsymbol{s}_j \\ V_2 &= \sum_{j=m,s}\left[\frac{1}{2}\mathrm{tr}\left(\tilde{\boldsymbol{\theta}}_j^{\mathrm{T}}\boldsymbol{\Gamma}_{j1}^{-1}\tilde{\boldsymbol{\theta}}_j\right) + \frac{\Gamma_{j2}^{-1}\tilde{D}_{j'}^2}{2} + \frac{\Gamma_{j3}^{-1}\tilde{\omega}_j^2}{2}\right] \\ V_3 &= \sum_{j=m,s}\eta_j\int_{t-\bar{d}_j}^{t}\frac{\bar{d}_j - t + \alpha}{\bar{d}_j}\boldsymbol{s}_j^{\mathrm{T}}(\alpha)\boldsymbol{s}_j(\alpha)\,\mathrm{d}\alpha\end{aligned} \tag{29}$$

with $\tilde{\boldsymbol{\theta}}_j = \boldsymbol{\theta}_j - \hat{\boldsymbol{\theta}}_j$, $\tilde{D}_{j'} = D_{j'} - \hat{D}_{j'}$, $\tilde{\omega}_j = \omega_j - \hat{\omega}_j$, $\eta_j \ge 0$ is a known constant.

First, the differentiation of V_1 can be described as

$$\dot{V}_1 = \textstyle\sum_{j=m,s}\left(\boldsymbol{s}_j^{\mathrm{T}}\boldsymbol{M}_j\dot{\boldsymbol{s}}_j + \frac{1}{2}\boldsymbol{s}_j^{\mathrm{T}}\dot{\boldsymbol{M}}_j\boldsymbol{s}_j\right). \tag{30}$$

Based on the description in (23) and the Property 2 of the teleoperation system, it can be obtained that

$$\begin{aligned}\dot{V}_1 &= \sum_{j=m,s}\boldsymbol{s}_j^{\mathrm{T}}\big[\boldsymbol{\tau}_j - \boldsymbol{f}_{he,j} + \boldsymbol{M}_{jo}\boldsymbol{\mu}_{j1} + \boldsymbol{M}_{jo}\boldsymbol{\mu}_{j2}\dot{d}_{j'} \\ &\quad + \boldsymbol{C}_{jo}\boldsymbol{\mu}_{j3} - \boldsymbol{G}_{jo} + \boldsymbol{\theta}_j^{\mathrm{T}}\boldsymbol{Y}_j(\boldsymbol{Z}_j) + \boldsymbol{\epsilon}_j\big] \\ &\le \sum_{j=m,s}\Big\{\boldsymbol{s}_j^{\mathrm{T}}\Big[\boldsymbol{\tau}_j + \boldsymbol{M}_{jo}\boldsymbol{\mu}_{j1} + \boldsymbol{C}_{jo}\boldsymbol{\mu}_{j3} - \boldsymbol{G}_{jo} + \boldsymbol{\theta}_j^{\mathrm{T}}\boldsymbol{Y}_j(\boldsymbol{Z}_j)\Big] \\ &\quad + |\boldsymbol{s}_j^{\mathrm{T}}\boldsymbol{M}_{jo}\boldsymbol{\mu}_{j2}||\dot{d}_{j'}| + \|\boldsymbol{s}_j\|\|\boldsymbol{\epsilon}_j - \boldsymbol{f}_{he,j}\|\Big\}.\end{aligned} \tag{31}$$

Therefore, with the Assumption 2, Remark 3, and Young's inequality (the detailed description of Young's inequality can

be found in Appendix-A), it can be obtained that

$$\begin{aligned}\dot{V}_1 \le & \sum_{j=m,s}\Big\{\boldsymbol{s}_j^{\mathrm{T}}\big[\boldsymbol{\tau}_j+\boldsymbol{M}_{jo}\boldsymbol{\mu}_{j1}+\boldsymbol{C}_{jo}\boldsymbol{\mu}_{j3}-\boldsymbol{G}_{jo}\\ &+\boldsymbol{\theta}_j^{\mathrm{T}}\boldsymbol{Y}_j(\boldsymbol{Z}_j)\big]+|\boldsymbol{s}_j^{\mathrm{T}}\boldsymbol{M}_{jo}\boldsymbol{\mu}_{j2}|D_{j'}+\|\boldsymbol{s}_j\|\omega_j\Big\}\\ \le & \sum_{j=m,s}\Big\{\boldsymbol{s}_j^{\mathrm{T}}\big[\boldsymbol{\tau}_j+\boldsymbol{M}_{jo}\boldsymbol{\mu}_{j1}+\boldsymbol{C}_{jo}\boldsymbol{\mu}_{j3}-\boldsymbol{G}_{jo}\\ &+\boldsymbol{\theta}_j^{\mathrm{T}}\boldsymbol{Y}_j(\boldsymbol{Z}_j)\big]+\frac{\boldsymbol{s}_j^{\mathrm{T}}\boldsymbol{s}_j\|\boldsymbol{M}_{jo}\boldsymbol{\mu}_{j2}\|^2}{2a_{j1}^2}D_{j'}\\ &+\frac{\boldsymbol{s}_j^{\mathrm{T}}\boldsymbol{s}_j}{2a_{j2}^2}\omega_j+\frac{a_{j1}^2+a_{j2}^2}{2}\Big\}. \end{aligned}\tag{32}$$

Then, with the control law in (26), it has

$$\begin{aligned}\dot{V}_1 \le & \sum_{j=m,s}\Bigg[-\boldsymbol{s}_j^{\mathrm{T}}\hat{\boldsymbol{\theta}}_j^{\mathrm{T}}\boldsymbol{Y}_j(\boldsymbol{Z}_j)-\frac{\boldsymbol{s}_j^{\mathrm{T}}\boldsymbol{s}_j\|\boldsymbol{M}_{jo}\boldsymbol{\mu}_{j2}\|^2}{2a_{j1}^2}\hat{D}_{j'}\\ &-\frac{\boldsymbol{s}_j^{\mathrm{T}}\boldsymbol{s}_j}{2a_{j2}^2}\hat{\omega}_j-\boldsymbol{s}_j^{\mathrm{T}}\boldsymbol{K}_{j1}\boldsymbol{s}_j-\boldsymbol{s}_j^{\mathrm{T}}\boldsymbol{K}_{j2}\mathrm{sig}(\boldsymbol{s}_j)^{\sigma}\\ &+\frac{\boldsymbol{s}_j^{\mathrm{T}}\boldsymbol{s}_j\|\boldsymbol{M}_{jo}\boldsymbol{\mu}_{j2}\|^2}{2a_{j1}^2}D_{j'}+\frac{\boldsymbol{s}_j^{\mathrm{T}}\boldsymbol{s}_j}{2a_{j2}^2}\omega_j+\frac{a_{j1}^2+a_{j2}^2}{2}\Bigg]\\ = & \sum_{j=m,s}\Big[-\boldsymbol{s}_j^{\mathrm{T}}\boldsymbol{K}_{j1}\boldsymbol{s}_j-\boldsymbol{s}_j^{\mathrm{T}}\boldsymbol{K}_{j2}\mathrm{sig}(\boldsymbol{s}_j)^{\sigma}+\boldsymbol{s}_j^{\mathrm{T}}\tilde{\boldsymbol{\theta}}_j^{\mathrm{T}}\boldsymbol{Y}_j(\boldsymbol{Z}_j)\\ &+\frac{\boldsymbol{s}_j^{\mathrm{T}}\boldsymbol{s}_j\|\boldsymbol{M}_{jo}\boldsymbol{\mu}_{j2}\|^2}{2a_{j1}^2}\tilde{D}_{j'}+\frac{\boldsymbol{s}_j^{\mathrm{T}}\boldsymbol{s}_j}{2a_{j2}^2}\tilde{\omega}_j+\frac{a_{j1}^2+a_{j2}^2}{2}\Big]. \end{aligned}\tag{33}$$

For V_2, based on the adaptive laws in (27), we can get that

$$\begin{aligned}\dot{V}_2 = & \sum_{j=m,s}\Big[\mathrm{tr}\Big(\tilde{\boldsymbol{\theta}}_j^{\mathrm{T}}\boldsymbol{\Gamma}_{j1}^{-1}\dot{\tilde{\boldsymbol{\theta}}}_j\Big)+\Gamma_{j2}^{-1}\tilde{D}_{j'}\dot{\tilde{D}}_{j'}+\Gamma_{j3}^{-1}\tilde{\omega}_j\dot{\tilde{\omega}}_j\Big]\\ = & \sum_{j=m,s}\Big[-\mathrm{tr}\Big(\tilde{\boldsymbol{\theta}}_j^{\mathrm{T}}\boldsymbol{\Gamma}_{j1}^{-1}\dot{\hat{\boldsymbol{\theta}}}_j\Big)-\Gamma_{j2}^{-1}\tilde{D}_{j'}\dot{\hat{D}}_{j'}-\Gamma_{j3}^{-1}\tilde{\omega}_j\dot{\hat{\omega}}_j\Big]\\ = & \sum_{j=m,s}\Big[-\mathrm{tr}\Big(\tilde{\boldsymbol{\theta}}_j^{\mathrm{T}}\boldsymbol{Y}_j(\boldsymbol{Z}_j)\boldsymbol{s}_j^{\mathrm{T}}\Big)+\mathrm{tr}\Big(\tilde{\boldsymbol{\theta}}_j^{\mathrm{T}}\boldsymbol{\Gamma}_{j1}^{-1}\hat{\boldsymbol{\theta}}_j\Big)\\ &-\frac{\tilde{D}_{j'}}{2a_{j1}^2}\boldsymbol{s}_j^{\mathrm{T}}\boldsymbol{s}_j\|\boldsymbol{M}_{jo}\boldsymbol{\mu}_{j2}\|^2+\Gamma_{j2}^{-1}\tilde{D}_{j'}\hat{D}_{j'}\\ &-\frac{\tilde{\omega}_j}{2a_{j2}^2}\boldsymbol{s}_j^{\mathrm{T}}\boldsymbol{s}_j+\Gamma_{j3}^{-1}\tilde{\omega}_j\hat{\omega}_j\Big]. \end{aligned}\tag{34}$$

For $\mathrm{tr}(\tilde{\boldsymbol{\theta}}_j^{\mathrm{T}}\boldsymbol{\Gamma}_{j1}^{-1}\hat{\boldsymbol{\theta}}_j)$, $\Gamma_{j2}^{-1}\tilde{D}_{j'}\hat{D}_{j'}$, and $\Gamma_{j3}^{-1}\tilde{\omega}_j\hat{\omega}_j$, the following inequalities are always established:

$$\begin{aligned}&\mathrm{tr}\Big(\tilde{\boldsymbol{\theta}}_j^{\mathrm{T}}\boldsymbol{\Gamma}_{j1}^{-1}\hat{\boldsymbol{\theta}}_j\Big)\le-\frac{1}{2}\mathrm{tr}\Big(\tilde{\boldsymbol{\theta}}_j^{\mathrm{T}}\boldsymbol{\Gamma}_{j1}^{-1}\tilde{\boldsymbol{\theta}}_j\Big)+\frac{1}{2}\mathrm{tr}\Big(\boldsymbol{\theta}_j^{\mathrm{T}}\boldsymbol{\Gamma}_{j1}^{-1}\boldsymbol{\theta}_j\Big)\\ &\Gamma_{j2}^{-1}\tilde{D}_{j'}\hat{D}_{j'}\le-\frac{\Gamma_{j2}^{-1}}{2}\tilde{D}_{j'}^2+\frac{\Gamma_{j2}^{-1}}{2}D_{j'}^2\\ &\Gamma_{j3}^{-1}\tilde{\omega}_j\hat{\omega}_j\le-\frac{\Gamma_{j3}^{-1}}{2}\tilde{\omega}_j^2+\frac{\Gamma_{j3}^{-1}}{2}\omega_j^2. \end{aligned}\tag{35}$$

With the presentation above, we have

$$\begin{aligned}\dot{V}_2 \le & \sum_{j=m,s}\Bigg[-\mathrm{tr}\Big(\tilde{\boldsymbol{\theta}}_j^{\mathrm{T}}\boldsymbol{Y}_j(\boldsymbol{Z}_j)\boldsymbol{s}_j^{\mathrm{T}}\Big)-\frac{\tilde{\omega}_j}{2a_{j2}^2}\boldsymbol{s}_j^{\mathrm{T}}\boldsymbol{s}_j\\ &-\frac{\tilde{D}_{j'}}{2a_{j1}}\boldsymbol{s}_j^{\mathrm{T}}\boldsymbol{s}_j\|\boldsymbol{M}_{jo}\boldsymbol{\mu}_{j2}\|^2\\ &-\frac{1}{2}\mathrm{tr}\Big(\tilde{\boldsymbol{\theta}}_j^{\mathrm{T}}\boldsymbol{\Gamma}_{j1}^{-1}\tilde{\boldsymbol{\theta}}_j\Big)-\frac{\Gamma_{j2}^{-1}}{2}\tilde{D}_{j'}^2-\frac{\Gamma_{j3}^{-1}}{2}\tilde{\omega}_j^2\\ &+\frac{1}{2}\mathrm{tr}\Big(\boldsymbol{\theta}_j^{\mathrm{T}}\boldsymbol{\Gamma}_{j1}^{-1}\boldsymbol{\theta}_j\Big)+\frac{\Gamma_{j2}^{-1}}{2}D_{j'}^2+\frac{\Gamma_{j3}^{-1}}{2}\omega_j^2\Bigg]. \end{aligned}\tag{36}$$

For V_3, we have

$$\dot{V}_3=\textstyle\sum_{j=m,s}\Big[\eta_j\boldsymbol{s}_j^{\mathrm{T}}\boldsymbol{s}_j-\frac{\eta_j}{\bar{d}_j}\int_{t-\bar{d}_j}^{t}\boldsymbol{s}_j^{\mathrm{T}}(\alpha)\boldsymbol{s}_j(\alpha)\,\mathrm{d}\alpha\Big].\tag{37}$$

In addition, it is clear that $\int_{t-\bar{d}_j}^{t}[(\bar{d}_j-t+\alpha)/\bar{d}_j]\boldsymbol{s}_j^{\mathrm{T}}(\alpha)\boldsymbol{s}_j(\alpha)\,\mathrm{d}\alpha \le \int_{t-\bar{d}_j}^{t}\boldsymbol{s}_j^{\mathrm{T}}(\alpha)\boldsymbol{s}_j(\alpha)\,\mathrm{d}\alpha$. Then we can get that

$$\dot{V}_3\le\textstyle\sum_{j=m,s}\Big[\eta_j\boldsymbol{s}_j^{\mathrm{T}}\boldsymbol{s}_j-\frac{\eta_j}{\bar{d}_j}\int_{t-\bar{d}_j}^{t}\frac{\bar{d}_j-t+\alpha}{\bar{d}_j}\boldsymbol{s}_j^{\mathrm{T}}(\alpha)\boldsymbol{s}_j(\alpha)\,\mathrm{d}\alpha\Big].\tag{38}$$

Finally, combining with the derivation of $\dot{V}_1$ in (33), $\dot{V}_2$ in (36), and $\dot{V}_3$ in (38), we can get that

$$\begin{aligned}\dot{V}\le & \sum_{j=m,s}\Bigg[-\boldsymbol{s}_j^{\mathrm{T}}\boldsymbol{K}_{j1}\boldsymbol{s}_j+\eta_j\boldsymbol{s}_j^{\mathrm{T}}\boldsymbol{s}_j-\boldsymbol{s}_j^{\mathrm{T}}\boldsymbol{K}_{j2}\mathrm{sig}(\boldsymbol{s}_j)^{\sigma}\\ &-\frac{1}{2}\mathrm{tr}\Big(\tilde{\boldsymbol{\theta}}_j^{\mathrm{T}}\boldsymbol{\Gamma}_{j1}^{-1}\tilde{\boldsymbol{\theta}}_j\Big)-\frac{\Gamma_{j2}^{-1}}{2}\tilde{D}_{j'}^2-\frac{\Gamma_{j3}^{-1}}{2}\tilde{\omega}_j^2\\ &-\frac{\eta_j}{\bar{d}_j}\int_{t-\bar{d}_j}^{t}\frac{\bar{d}_j-t+\alpha}{\bar{d}_j}\boldsymbol{s}_j^{\mathrm{T}}(\alpha)\boldsymbol{s}_j(\alpha)\,\mathrm{d}\alpha+\Xi_j\Bigg]\\ \le & \sum_{j=m,s}\Bigg[-\frac{k_{j1}}{2}\boldsymbol{s}_j^{\mathrm{T}}\boldsymbol{M}_j\boldsymbol{s}_j-\frac{1}{2}\mathrm{tr}\Big(\tilde{\boldsymbol{\theta}}_j^{\mathrm{T}}\boldsymbol{\Gamma}_{j1}^{-1}\tilde{\boldsymbol{\theta}}_j\Big)\\ &-\frac{\Gamma_{j2}^{-1}}{2}\tilde{D}_{j'}^2-\frac{\Gamma_{j3}^{-1}}{2}\tilde{\omega}_j^2\\ &-\frac{\eta_j}{\bar{d}_j}\int_{t-\bar{d}_j}^{t}\frac{\bar{d}_j-t+\alpha}{\bar{d}_j}\boldsymbol{s}_j^{\mathrm{T}}(\alpha)\boldsymbol{s}_j(\alpha)\,\mathrm{d}\alpha+\Xi_j\Bigg]. \end{aligned}\tag{39}$$

where $k_{j1}=[2\lambda_{\min}(\boldsymbol{K}_{j1})-2\eta_j/(\lambda_{\min}(\boldsymbol{M}_{j1}))]$, and $\Xi_j=(1/2)\mathrm{tr}(\boldsymbol{\theta}_j^{\mathrm{T}}\boldsymbol{\Gamma}_{j1}^{-1}\boldsymbol{\theta}_j)+(\Gamma_{j2}^{-1}/2)D_{j'}^2+(\Gamma_{j3}^{-1}/2)\omega_j^2+[(a_{j1}^2+a_{j2}^2)/2]$ is a positive constant. The $\lambda_{\min}(\bullet)$ and $\lambda_{\max}(\bullet)$ represent the minimun and maximum eigenvalues of the matrix $\bullet$, respectively. It is necessary to set the approximate $\boldsymbol{K}_{j1}$ to make $k_{j1}>0$, or in other words, there exists a small value of η_j to make $k_{j1}>0$.

Then define $\Lambda=\min(k_{j1},1,1/d_j)$ and $\Xi=\Xi_m+\Xi_s$, it is obvious that $\Lambda>0$ and $\Xi>0$, we can obtain $\dot{V}$ as

$$\dot{V}\le-\Lambda V+\Xi\tag{40}$$

which implies that [56]

$$V(t)\le\Big(V(0)-\frac{\Xi}{\Lambda}\Big)e^{-\Lambda t}+\frac{\Xi}{\Lambda}.\tag{41}$$

Thus, we have $V(t)\to\Xi/\Lambda$ when $t\to\infty$, and $V(t)$ is bounded. Since V is radically consisted with $\boldsymbol{s}_j$, $\tilde{\boldsymbol{\theta}}_j$, $\tilde{D}_{j'}$, and $\tilde{\omega}_j$, it can imply that $\boldsymbol{s}_j$, $\tilde{\boldsymbol{\theta}}_j$, $\tilde{D}_{j'}$, and $\tilde{\omega}_j$ are all bounded.

The stability analysis mentioned above shows that the closed-loop system is asymptotically stable and the signals are bounded. Then the analysis of finite-time performance is represented as follows.

Taking the Lyapunov candidate function as $\bar{V} = V_1 + V_2$, thus similar to the (33) and (36), there exists

$$\begin{aligned}\dot{\bar{V}} \le \sum_{j=m,s}\Bigg[&-\boldsymbol{s}_j^{\mathrm{T}}\boldsymbol{K}_{j1}\boldsymbol{s}_j - \frac{1}{2}\mathrm{tr}\Big(\tilde{\boldsymbol{\theta}}_j^{\mathrm{T}}\boldsymbol{\Gamma}_{j1}^{-1}\tilde{\boldsymbol{\theta}}_j\Big) - \frac{\Gamma_{j2}^{-1}}{2}\tilde{D}_{j'}^2 \\ &-\frac{\Gamma_{j3}^{-1}}{2}\tilde{\omega}_j^2 - \boldsymbol{s}_j^{\mathrm{T}}\boldsymbol{K}_{j2}\mathrm{sig}(\boldsymbol{s}_j)^{\sigma} - \left(\frac{\Gamma_{j2}^{-1}}{2}\tilde{D}_{j'}^2\right)^{\frac{\sigma+1}{2}} \\ &-\left(\frac{1}{2}\mathrm{tr}\Big(\tilde{\boldsymbol{\theta}}_j^{\mathrm{T}}\boldsymbol{\Gamma}_{j1}^{-1}\tilde{\boldsymbol{\theta}}_j\Big)\right)^{\frac{\sigma+1}{2}} - \left(\frac{\Gamma_{j3}^{-1}}{2}\tilde{\omega}_j^2\right)^{\frac{\sigma+1}{2}} \\ &+\left(\frac{1}{2}\mathrm{tr}\Big(\tilde{\boldsymbol{\theta}}_j^{\mathrm{T}}\boldsymbol{\Gamma}_{j1}^{-1}\tilde{\boldsymbol{\theta}}_j\Big)\right)^{\frac{\sigma+1}{2}} + \left(\frac{\Gamma_{j2}^{-1}}{2}\tilde{D}_{j'}^2\right)^{\frac{\sigma+1}{2}} \\ &+\left(\frac{\Gamma_{j3}^{-1}}{2}\tilde{\omega}_j^2\right)^{\frac{\sigma+1}{2}} + \Xi_j\Bigg]. \end{aligned} \tag{42}$$

We define $\bar{k}_{j1} = \lambda_{\min}(\boldsymbol{K}_{j1})$, $\bar{k}_{j2} = \lambda_{\min}(\boldsymbol{K}_{j2})$, and $\bar{\Xi}_j = ((1/2)\mathrm{tr}(\tilde{\boldsymbol{\theta}}_j^{\mathrm{T}}\boldsymbol{\Gamma}_{j1}^{-1}\tilde{\boldsymbol{\theta}}_j))^{(\sigma+1/2)} + ((\Gamma_{j2}^{-1}/2)\tilde{D}_{j'}^2)^{[(\sigma+1)/2]} + ((\Gamma_{j3}^{-1}/2)\tilde{\omega}_j^2)^{[(\sigma+1)/2]} + \Xi_j$. With the boundness of $\tilde{\boldsymbol{\theta}}_j$, $\tilde{D}_{j'}$, and $\tilde{\omega}_j$ we have analyzed above, it is obvious that $\bar{\Xi}_j$ is also bounded. Thus, for $j = m, s$, there exists the positive constants Υ_m and Υ_s such that $0 \le \bar{\Xi}_m \le \Upsilon_m$ and $0 \le \bar{\Xi}_s \le \Upsilon_s$, respectively. Then the $\dot{\bar{V}}$ can be represented as

$$\begin{aligned}\dot{\bar{V}} \le \sum_{j=m,s}\Bigg[&-\bar{k}_{j1}\boldsymbol{s}_j^{\mathrm{T}}\boldsymbol{s}_j - \frac{1}{2}\mathrm{tr}\Big(\tilde{\boldsymbol{\theta}}_j^{\mathrm{T}}\boldsymbol{\Gamma}_{j1}^{-1}\tilde{\boldsymbol{\theta}}_j\Big) - \frac{\Gamma_{j2}^{-1}}{2}\tilde{D}_{j'}^2 \\ &-\frac{\Gamma_{j3}^{-1}}{2}\tilde{\omega}_j^2 - \bar{k}_{j2}\Big(\boldsymbol{s}_j^{\mathrm{T}}\boldsymbol{s}_j\Big)^{\frac{\sigma+1}{2}} - \left(\frac{\mathrm{tr}\Big(\tilde{\boldsymbol{\theta}}_j^{\mathrm{T}}\boldsymbol{\Gamma}_{j1}^{-1}\tilde{\boldsymbol{\theta}}_j\Big)}{2}\right)^{\frac{\sigma+1}{2}} \\ &-\left(\frac{\Gamma_{j2}^{-1}}{2}\tilde{D}_{j'}^2\right)^{\frac{\sigma+1}{2}} - \left(\frac{\Gamma_{j3}^{-1}}{2}\tilde{\omega}_j^2\right)^{\frac{\sigma+1}{2}} + \frac{\Upsilon_j\boldsymbol{s}_j^{\mathrm{T}}\boldsymbol{s}_j}{2\|\boldsymbol{s}_j\|^2} \\ &+\frac{\Upsilon_j\Big(\boldsymbol{s}_j^{\mathrm{T}}\boldsymbol{s}_j\Big)^{\frac{\sigma+1}{2}}}{2\|\boldsymbol{s}_j\|^{\sigma+1}}\Bigg] \\ =\sum_{j=m,s}\Bigg[&-\left(\bar{k}_{j1} - \frac{\Upsilon_j}{2\|\boldsymbol{s}_j\|^2}\right)\boldsymbol{s}_j^{\mathrm{T}}\boldsymbol{s}_j - \frac{1}{2}\mathrm{tr}\Big(\tilde{\boldsymbol{\theta}}_j^{\mathrm{T}}\boldsymbol{\Gamma}_{j1}^{-1}\tilde{\boldsymbol{\theta}}_j\Big) \\ &-\frac{\Gamma_{j2}^{-1}}{2}\tilde{D}_{j'}^2 - \frac{\Gamma_{j3}^{-1}}{2}\tilde{\omega}_j^2 - \left(\bar{k}_{j2} - \frac{\Upsilon_j}{2\|\boldsymbol{s}_j\|^{\sigma+1}}\right)\Big(\boldsymbol{s}_j^{\mathrm{T}}\boldsymbol{s}_j\Big)^{\frac{\sigma+1}{2}} \\ &-\left(\frac{\mathrm{tr}\Big(\tilde{\boldsymbol{\theta}}_j^{\mathrm{T}}\boldsymbol{\Gamma}_{j1}^{-1}\tilde{\boldsymbol{\theta}}_j\Big)}{2}\right)^{\frac{\sigma+1}{2}} - \left(\frac{\Gamma_{j2}^{-1}}{2}\tilde{D}_{j'}^2\right)^{\frac{\sigma+1}{2}} \\ &-\left(\frac{\Gamma_{j3}^{-1}}{2}\tilde{\omega}_j^2\right)^{\frac{\sigma+1}{2}}\Bigg]. \end{aligned} \tag{43}$$

Then we can get that

$$\begin{aligned}\dot{\bar{V}} \le \sum_{j=m,s}\Bigg[&-\frac{2\Big(\bar{k}_{j1} - \frac{\Upsilon_j}{2\|\boldsymbol{s}_j\|^2}\Big)}{\lambda_{\max}(\boldsymbol{M}_j)}\frac{1}{2}\boldsymbol{s}_j^{\mathrm{T}}\boldsymbol{M}_j\boldsymbol{s}_j - \frac{\Gamma_{j2}^{-1}}{2}\tilde{D}_{j'}^2 \\ &-\frac{1}{2}\mathrm{tr}\Big(\tilde{\boldsymbol{\theta}}_j^{\mathrm{T}}\boldsymbol{\Gamma}_{j1}^{-1}\tilde{\boldsymbol{\theta}}_j\Big) - \frac{\Gamma_{j3}^{-1}}{2}\tilde{\omega}_j^2 \\ &-\frac{2^{\frac{\sigma+1}{2}}\Big(\bar{k}_{j2} - \frac{\Upsilon_j}{2\|\boldsymbol{s}_j\|^{\sigma+1}}\Big)}{\big(\lambda_{\max}(\boldsymbol{M}_j)\big)^{\frac{\sigma+1}{2}}}\left(\frac{1}{2}\boldsymbol{s}_j^{\mathrm{T}}\boldsymbol{M}_j\boldsymbol{s}_j\right)^{\frac{\sigma+1}{2}} \\ &-\left(\frac{1}{2}\mathrm{tr}\Big(\tilde{\boldsymbol{\theta}}_j^{\mathrm{T}}\boldsymbol{\Gamma}_{j1}^{-1}\tilde{\boldsymbol{\theta}}_j\Big)\right)^{\frac{\sigma+1}{2}} - \left(\frac{\Gamma_{j2}^{-1}}{2}\tilde{D}_{j'}^2\right)^{\frac{\sigma+1}{2}} \\ &-\left(\frac{\Gamma_{j3}^{-1}}{2}\tilde{\omega}_j^2\right)^{\frac{\sigma+1}{2}}\Bigg] \\ \le -\bar{\Lambda}_1\bar{V} - \bar{\Lambda}_2\bar{V}^{\frac{\sigma+1}{2}}& \end{aligned} \tag{44}$$

where for $j = m, s$

$$\begin{aligned}\bar{\Lambda}_1 &= \min\left[\frac{2\Big(\bar{k}_{j1} - \frac{\Upsilon_j}{2\|\boldsymbol{s}_j\|^2}\Big)}{\lambda_{\max}(\boldsymbol{M}_j)}, 1\right] \\ \bar{\Lambda}_2 &= \min\left[\frac{2^{\frac{\sigma+1}{2}}\Big(\bar{k}_{j2} - \frac{\Upsilon_j}{2\|\boldsymbol{s}_j\|^{\sigma+1}}\Big)}{\big(\lambda_{\max}(\boldsymbol{M}_j)\big)^{\frac{\sigma+1}{2}}}, 1\right]. \end{aligned} \tag{45}$$

Note that it is needed to set the larger values of $\boldsymbol{K}_{j1}$ and $\boldsymbol{K}_{j1}$ to make $\bar{\Lambda}_1, \bar{\Lambda}_2 > 0$.

We define the region Ψ_j as $\Psi_j = \min(\Psi_{j1}, \Psi_{j2})$, where $\Psi_{j1} = \sqrt{(\Upsilon_j/2\bar{k}_{j1})}$, $\Psi_{j2} = \sqrt{[\sigma+1][\Upsilon_j/(2^{(\sigma+1/2)})]\bar{k}_{j2}}$. It implies that if $\|\boldsymbol{s}_j\| > \Psi_j$, it has $\dot{\bar{V}} + \bar{\Lambda}_1\bar{V} + \bar{\Lambda}_2\bar{V}^{(\sigma+1/2)} \le 0$, which means the system is finite-time stable and $\boldsymbol{s}_j$ can converge to the region Ψ_j in finite-time. Based on the Lemma 2, the reaching time T can be given by

$$T \le \frac{2}{\bar{\Lambda}_1(1-\sigma)}\ln\frac{\bar{\Lambda}_1\bar{V}^{\frac{1-\sigma}{2}}(0) + \bar{\Lambda}_2}{\bar{\Lambda}_2}. \tag{46}$$

This completes the proof. ■

Remark 5: Based on Theorem 1, for $j = m, s$, the approximate control gains can be selected according to the following rules.

1) First, the filter parameters $\boldsymbol{L}_{j1}$ and $\boldsymbol{L}_{j2}$ in (8) and (16) are all positive-definite diagonal matrices. The smaller $\boldsymbol{L}_{j1}$ and $\boldsymbol{L}_{j2}$ would have smoother output of filters (the input signals are the angular velocity and force signal transmitted through the time-varying delay).
2) Then, the gains in auxiliary error system $\boldsymbol{\eta}_{j1}$ and $\boldsymbol{\eta}_{j2}$, can be given. The values of $\boldsymbol{\eta}_{j1}$ and $\boldsymbol{\eta}_{j2}$ are all positive-definite diagonal matrices and represent the weights of position error and force error in the error system.
3) Next, the parameters $\boldsymbol{\lambda}_{j1}$, $\boldsymbol{\lambda}_{j2}$, η_{j1}, and η_{j2} in auxiliary variable $\boldsymbol{s}_j$ can be given according to the system output performance. In addition, they should meet $\boldsymbol{\lambda}_{j1}$ and $\boldsymbol{\lambda}_{j2}$ are positive-definite diagonal matrices, $1 < \sigma_{j1} < 2$, and $0 < \sigma_{j2} < 1$.

4) $\boldsymbol{K}_{j1}$ and $\boldsymbol{K}_{j2}$ are positive-definite diagonal matrices, a_{j1} and a_{j2} are positive constants. In addition, bigger $\boldsymbol{K}_{j1}, \boldsymbol{K}_{j2}$ and smaller a_{j1}, a_{j2} can get the smaller convergence domain of $\boldsymbol{s}_j$.
5) $\boldsymbol{\Gamma}_{j1}$ is the positive diagonal matrix and $\Gamma_{j2}, \Gamma_{j3} > 0$. $0 < \sigma < 1$.

V. Simulation Analysis

In this section, we design the simulation experiment to validate the effectiveness of our proposed control method. Some simulations are performed in MATLAB/Simulink environment to evaluate our proposed control method. A pair of 2-DOF revolute joint manipulators are applied as the master and slave robots in the simulated teleoperation system. The dynamics of master and slave robot are the same as (1), the description of mass inertia matrix $\boldsymbol{M}_j$, centripetal-coriolis matrix $\boldsymbol{C}_j$, and gravitational torque $\boldsymbol{G}_j$ can be attained in [57]. The vector of friction torque $\boldsymbol{B}_j$ is given as

$$\boldsymbol{B}_j = \left[b_{j1}\dot{\boldsymbol{q}}_{j1} + b_{j2}\text{sign}\left(\dot{\boldsymbol{q}}_{j1}\right), b_{j3}\dot{\boldsymbol{q}}_{j2} + b_{j4}\text{sign}\left(\dot{\boldsymbol{q}}_{j2}\right)\right]^{\text{T}}.$$

The parameters of master and slave robots, which are used for the simulation, are chosen as $m_{m1} = m_{s1} = 3.5$kg, $m_{m2} = m_{s2} = 2.5$kg, $l_{m1} = l_{s1} = 0.3$m, $l_{m2} = l_{s2} = 0.35$m, $b_{m1} = b_{m3} = 0.5$, $b_{m2} = b_{m4} = 0.2$, $b_{s1} = b_{s2} = b_{s3} = b_{s4} = 0.3$, $g = 9.8\text{m/s}^2$. The damping and spring matrices in operator model are $\boldsymbol{D}_h = \text{diag}(0.1, 0.1)$ and $\boldsymbol{S}_h = \text{diag}(10.0, 10.0)$. The damping and spring matrices in environment model are $\boldsymbol{D}_e = \text{diag}(0.5, 0.5)$ and $\boldsymbol{S}_e = \text{diag}(10.0, 10.0)$. The uncertain dynamics of teleoperation system are, respectively, defined as $\Delta\boldsymbol{M}_j = 0.02\sin(4t)\boldsymbol{M}_j$, $\Delta\boldsymbol{C}_j = 0.02\sin(4t)\boldsymbol{C}_j$, $\Delta\boldsymbol{G}_j = 0.02\sin(4t)\boldsymbol{G}_j$. The master–slave time-varying communication delays $d_m(t), d_s(t)$ and the external operator interference torque $\boldsymbol{f}_h$ are shown in Fig. 2. The time-varying delay signals are obtained by superimposing the random signals on the sinusoidal signals. $\boldsymbol{f}_h$ only has the interference torque in the x-direction, the torque value is 0 in the y-direction. The external torque of the environment is 0 in both directions. The initial conditions of joint positions are set as $\boldsymbol{q}_m = [\pi/12, \pi/12]^{\text{T}}$, $\dot{\boldsymbol{q}}_m = [0, 0]^{\text{T}}$, $\boldsymbol{q}_s = [\pi/4, \pi/6]^{\text{T}}$, and $\dot{\boldsymbol{q}}_s = [0, 0]^{\text{T}}$. Then the master–slave dynamic descriptions, the dynamic uncertainties, the operator and the environment models, and the models of asymmetric time-varying communication delay are all established.

The parameters of nominal models $\boldsymbol{M}_{jo}$, $\boldsymbol{C}_{jo}$, and $\boldsymbol{G}_{jo}$ are set as $m_{mo1} = m_{mo2} = m_{so1} = m_{so2} = 2.0$kg, $l_{mo1} = l_{mo2} = l_{so1} = l_{so2} = 0.3$m. The parameters of master controller are defined as $\boldsymbol{L}_{m1} = \text{diag}(0.8, 0.8)$, $\boldsymbol{L}_{m2} = \text{diag}(0.1, 0.1)$, $\boldsymbol{\eta}_{m1} = \text{diag}(1, 1)$, $\boldsymbol{\eta}_{m2} = \text{diag}(0.02, 0.02)$, $\boldsymbol{\lambda}_{m1} = \text{diag}(1.98, 1.98)$, $\boldsymbol{\lambda}_{m2} = \text{diag}(0.72, 0.72)$, $\sigma_{m1} = 1.1$, $\sigma_{m2} = 0.95$, $\sigma = 0.8$, $a_{m1} = 0.5$, $a_{m2} = 0.5$, $\boldsymbol{K}_{m1} = \text{diag}(15, 15)$, $\boldsymbol{K}_{m2} = \text{diag}(15, 15)$, $\boldsymbol{\Gamma}_{m1} = \text{diag}(0.6, 0.6)$, $\Gamma_{m2} = \Gamma_{m3} = 0.6$. The parameters of slave controller are set as $\boldsymbol{L}_{s1} = \text{diag}(0.8, 0.8)$, $\boldsymbol{L}_{s2} = \text{diag}(0.1, 0.1)$, $\boldsymbol{\eta}_{s1} = \text{diag}(1, 1)$, $\boldsymbol{\eta}_{s2} = \text{diag}(0.02, 0.02)$, $\boldsymbol{\lambda}_{s1} = \text{diag}(1.98, 1.98)$, $\boldsymbol{\lambda}_{s2} = \text{diag}(0.72, 0.72)$, $\sigma_{s1} = 1.1$, $\sigma_{s2} = 0.95$, $a_{s1} = 0.5$, $a_{s2} = 0.5$, $\boldsymbol{K}_{s1} = \text{diag}(15, 15)$, $\boldsymbol{K}_{s2} = \text{diag}(15, 15)$, $\boldsymbol{\Gamma}_{s1} = \text{diag}(0.6, 0.6)$, $\Gamma_{s2} = \Gamma_{s3} = 0.6$. For RBFNN, $j = m, s$, the number of hidden layer nodes is 5, the width of Gaussian function $b_j = 4$, the center vector of Gaussian function from the 1-st node to the 5-th node are $c_{j1}^{\text{T}} = -4\times\text{ones}(10, 1)$, $c_{j2}^{\text{T}} = -2\times\text{ones}(10, 1)$, $c_{j3}^{\text{T}} = 0\times\text{ones}(10, 1)$, $c_{j4}^{\text{T}} = 2\times\text{ones}(10, 1)$, and $c_{j5}^{\text{T}} = 4\times\text{ones}(10, 1)$, respectively.

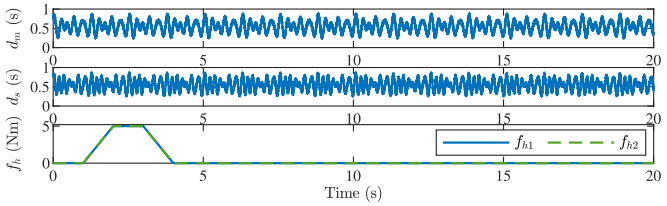

Fig. 2. Communication time delays $d_m(t)$, $d_s(t)$, and external operator torque $\boldsymbol{f}_h$ for simulation.

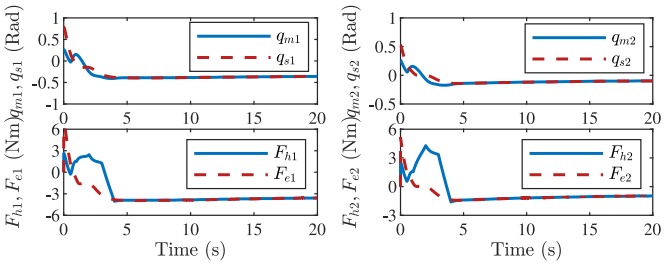

Fig. 3. Joint position of master and slave robots $\boldsymbol{q}_m$, $\boldsymbol{q}_s$; human and environment forces $\boldsymbol{F}_h$, $\boldsymbol{F}_e$.

A. Stability and Tracking Performance Verification

The first simulation set is used to illustrate the stability and the position/force tracking performance of the closed-loop teleoperation system. The simulation results under above simulation conditions are shown in Figs. 3–8. Fig. 3 shows the position curves of master and slave robots and force curves of human operator and environment with time-varying delays and external human operator torque in Fig. 2. To better illustrate the effects of position and force tracking between master and slave side, Figs. 4 and 5 are given to present the position tracking and force tracking errors, respectively. It can be seen that the teleoperation system with proposed control scheme has a good position and force tracking performance. It is further verified that the position and torque tracking errors can converge into a very small neighbor with time-varying delays and uncertain dynamics.

Furthermore, based on the proof of Theorem 1, it can be obtained that $\boldsymbol{s}_j$, $\tilde{\boldsymbol{\theta}}_j$, $\tilde{D}_{j'}$, and $\tilde{\omega}_j$ are all bounded, for $j = m, s$. Therefore, Fig. 6 shows the adaptive variables $\hat{\boldsymbol{\theta}}_j$, $\hat{D}_j$, and $\hat{\omega}_j$ in controller. It is evident that the above adaptive parameters $\hat{\boldsymbol{\theta}}_j$, $\hat{D}_j$, and $\hat{\omega}_j$ are all bounded, which can infer the boundedness of $\tilde{\boldsymbol{\theta}}_j$, $\tilde{D}_j$, and $\tilde{\omega}_j$. The norm curves of the designed auxiliary variables $\boldsymbol{s}_m$ and $\boldsymbol{s}_s$ are also given in Fig. 7, and the boundness of $\boldsymbol{s}_j$ can be verified. The control torque $\boldsymbol{\tau}_m$ and $\boldsymbol{\tau}_s$ are presented in Fig. 8. All of these results show the stability and position/force tracking performance of the teleoperation system wit our proposed control scheme.

B. Comparisons With Other Control Methods

In order to illustrate the effectiveness of the proposed control algorithm, the simulation comparisons with other related

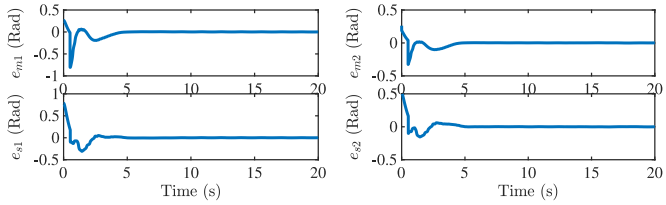

Fig. 4. Position tracking errors of master and slave robots.

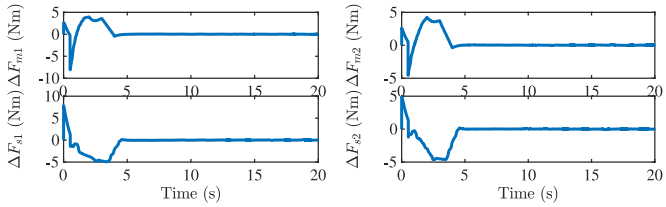

Fig. 5. Force tracking errors of master and slave robots.

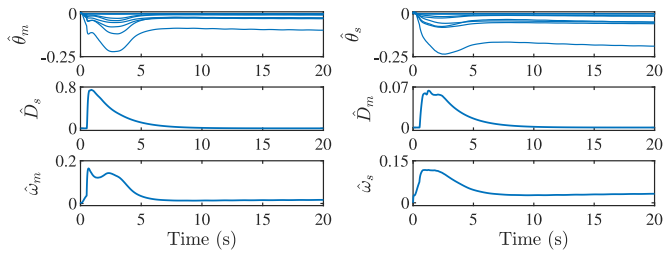

Fig. 6. Adaptive RBFNN parameters $\hat{\boldsymbol{\theta}}_m$, $\hat{\boldsymbol{\theta}}_s$, and adaptive parameters $\hat{D}_m$, $\hat{D}_s$, $\hat{\omega}_m$, and $\hat{\omega}_s$.

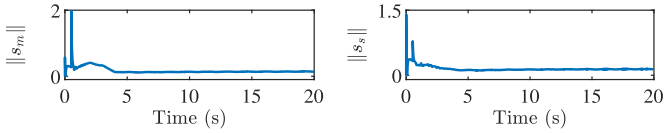

Fig. 7. Norm values of $\boldsymbol{s}_m$ and $\boldsymbol{s}_s$.

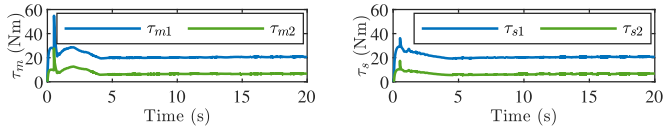

Fig. 8. Control torques of master and slave robots.

control methods in [46]–[49] are also implemented. The comparison of simulation results is set to two parts. The study is carried out by comparing the convergence speed and the steady-state performance of tracking errors with the different control methods. The simulation settings are the same for all control methods.

In part 1, the comparison study between nonfinite-time control schemes in [46] (method 1), [47] (method 2), and this work is performed. In [46], a PD control method with force tracking compensation is investigated to get the asymptotic convergence of position and force tracking. In [47], a nonlinear-proportional plus nonlinear damping (nP+nD) controller with environment torque compensation is proposed. Fig. 9 gives the curves of position synchronization errors with method 1, method 2, and proposed methods. Fig. 10 shows the force tracking error curves with method 1, method 2, and proposed methods. From

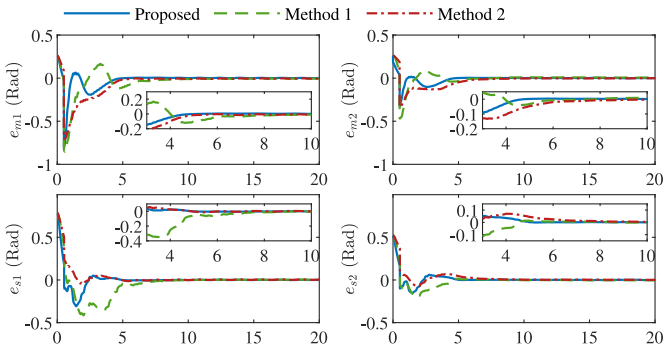

Fig. 9. Comparison of position tracking performance with the proposed method and methods 1 and 2.

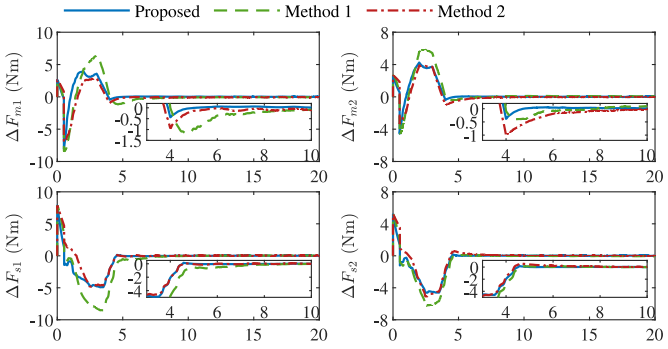

Fig. 10. Comparison of force tracking with our proposed method and methods 1 and 2.

which, it can be found that the proposed finite-time control algorithm has a faster convergence speed than the methods in [46] and [47]. This can further explain that the finite-time control structure has the faster convergence speed than infinite-time control methods.

In [48] and our previous work [49], the position and force tracking errors are used to design auxiliary variables for position and force tracking control, which has the similar idea to this work. In addition, the auxiliary variables and controller structure in [48] is different, and the controllers in [48] and [49] are not finite-time control structure. Therefore, in part 2, the comparison analysis between the control methods in [48] (method 3), [49] (method 4), and this work is performed to analyze the characteristics of them. The position and force tracking error curves of method 3, method 4, and proposed are shown in Figs. 11 and 12. It can be seen that the error convergence performance in [48] is worse than the proposed finite-time method. Meanwhile, it is shown that the error curve based on method 4 has a small oscillation in convergence process (such as $\boldsymbol{e}_{m1}$, $\boldsymbol{e}_{s1}$, $\Delta\boldsymbol{F}_{m1}$, and $\Delta\boldsymbol{F}_{s1}$), which increases its convergence time.

To better illustrate the steady-state performance of these control methods, root mean square error (RMSE) index is used to quantify the position and force tracking errors during 10 s–20 s. The RMSE values of position tracking and force tracking are shown in Tables II and IV, respectively. One can find that the RMSEs of position and force errors with proposed control method are smaller than the other four control methods, which means the proposed controller has the better steady-state performance.

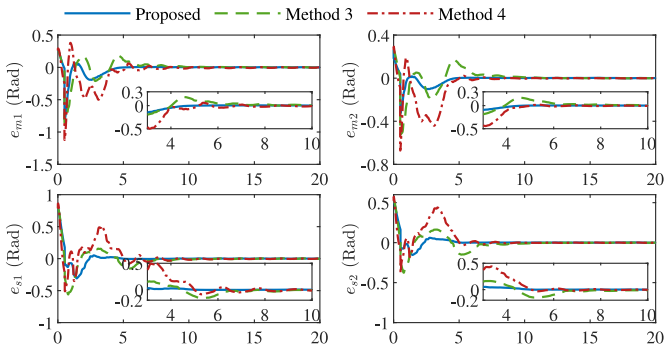

Fig. 11. Comparison of position tracking errors with the proposed control scheme and methods 3 and 4.

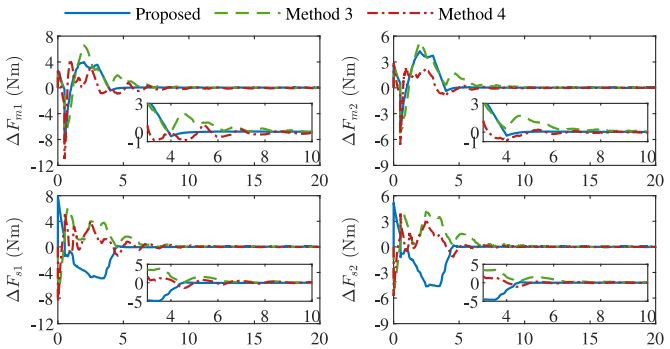

Fig. 12. Comparison of torque tracking with the proposed method and methods 3 and 4.

TABLE I
COMPARISON OF POSITION TRACKING ERROR'S RMSE WITH DIFFERENT CONTROL METHODS DURING 10–20 S

RMSE	Proposed	Method 1	Method 2	Method 3	Method 4
$\boldsymbol{e}_{m1}$	**0.0022**	0.0036	0.0064	0.0058	0.0054
$\boldsymbol{e}_{m2}$	0.0015	0.0022	0.0085	0.0024	**0.0014**
$\boldsymbol{e}_{s1}$	**0.0014**	0.0044	0.0029	0.0038	0.0054
$\boldsymbol{e}_{s2}$	**0.0011**	0.0028	0.0030	0.0029	0.0018

TABLE II
COMPARISON OF FORCE TRACKING ERROR'S RMSE WITH DIFFERENT CONTROL METHODS DURING 10–20 S

RMSE	Proposed	Method 1	Method 2	Method 3	Method 4
$\Delta\boldsymbol{F}_{m1}$	**0.0214**	0.0350	0.0620	0.0569	0.0534
$\Delta\boldsymbol{F}_{m2}$	**0.0143**	0.0231	0.0830	0.0252	**0.0143**
$\Delta\boldsymbol{F}_{s1}$	**0.0144**	0.0458	0.0288	0.0383	0.0548
$\Delta\boldsymbol{F}_{s2}$	**0.0116**	0.0278	0.0284	0.0299	0.0202

VI. EXPERIMENT ANALYSIS

In this section, the experiments are achieved to verify the validity of the proposed control method. The experimental platform is composed of two PHANToM Omni devices. These devices run in MATLAB/Simulink environment based on S-Function and OpenHaptics SDK functions. The experimental teleoperation system is shown in Fig. 13.

The PHANToM Omni robot is a small haptic device, it contains three actuated revolute joints and three passive revolute joints. We used the first three actuated joints of PHANToM Omni for the experiment. The end grips of these two robots are in the fixed state. The dynamic descriptions and the model parameters in our experiment have been borrowed from [52]. Two experimental schemes as free motion and force contact are designed to better verify the superiority of the proposed method. The time delays of the system are the same as the setting in the above simulation part. The RBFNN is used to estimate the unknown dynamic and uncertainties of the system. The width of Gaussian function are set as $b_j = 1.5$, and the center values of Gaussian functions are $c = [-5, -2.5, 0, 2.5, 5]$.

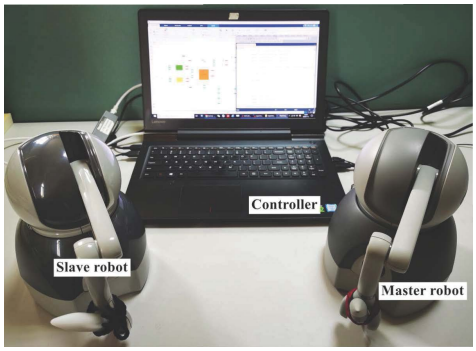

Fig. 13. Teleoperation system for experiment in our work.

In addition, the parameters of master and slave controllers are set as $\boldsymbol{L}_{m1} = \boldsymbol{L}_{m2} = \boldsymbol{L}_{s1} = \boldsymbol{L}_{s2} = \text{diag}(0.1, 0.1, 0.1)$, $\boldsymbol{\eta}_{m1} = \boldsymbol{\eta}_{s1} = \text{diag}(0.9, 0.9, 0.9)$, $\boldsymbol{\eta}_{m2} = \boldsymbol{\eta}_{s2} = \text{diag}(0.1, 0.1, 0.1)$, $\boldsymbol{\lambda}_{m1} = \boldsymbol{\lambda}_{s1} = \text{diag}(50, 50, 50)$, $\boldsymbol{\lambda}_{m2} = \boldsymbol{\lambda}_{s2} = \text{diag}(35, 45, 45)$, $\sigma_{m1} = \sigma_{s1} = 1.2$, $\sigma_{m2} = \sigma_{s2} = 0.9$, $\sigma = 0.3$, $a_{m1} = a_{m2} = a_{s1} = a_{s2} = 5$, $\boldsymbol{K}_{m1} = \boldsymbol{K}_{m2} = \boldsymbol{K}_{s1} = \boldsymbol{K}_{s2} = \text{diag}(70, 90, 90)$, $\boldsymbol{\Gamma}_{m1} = \boldsymbol{\Gamma}_{s1} = \text{diag}(0.9, 0.9, 0.9)$, $\Gamma_{m2} = \Gamma_{m3} = \Gamma_{s2} = \Gamma_{s3} = 0.9$.

A. Free Motion

In this section, the slave robot is performed in fine free state and the operator's torque on the master robot is not introduced into the controller. Our target is to verify that the proposed control scheme is still effective when the slave robot is in the free motion. Operator does not need to feel large force feedback. Fig. 14 shows the performance of the system with dynamic unknown and varying time-delays. It is obvious that the slave robot can still track the joint position of the master robot when ignoring the operator and environmental torques. In addition, the proposed control method is compared with the other two nonfinite-time methods in [47] (case 1) and [49] (case 2). Figs. 15 and 16 show the position performance of the system in free motion with case 1 and case 2. It can be seen that the position tracking performance is weak. Especially for the second joint of slave robot, the position of master robot is unable to be well tracked. The RMSEs of position tracking errors in Figs. 14–16 are listed in Table III to better demonstrate tracking performance with different methods. It can be seen that the RMSE values of the proposed method are smaller than the other two methods. This indicates that the proposed finite-time control system can achieve more accurate and fast position synchronization when the slave robot is not in contact with the environment.

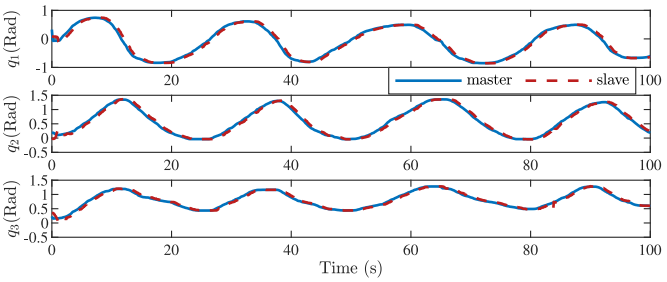

Fig. 14. Joint position tracking with proposed method in free motion.

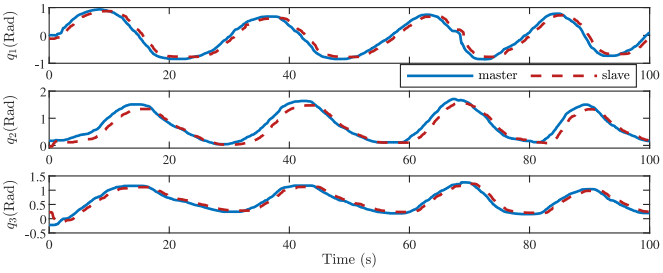

Fig. 15. Joint position tracking with case 1 in free motion.

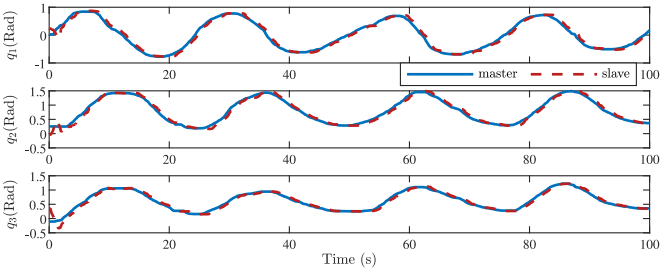

Fig. 16. Joint position tracking with case 2 in free motion.

TABLE III
RMSE OF POSITION TRACKING ERROR IN FREE MOTION

RMSE	Proposed	Case 1	Case 2
Joint1	**0.0561**	0.1386	0.0964
Joint2	**0.0502**	0.1746	0.0832
Joint3	**0.0354**	0.0995	0.0760

B. Force Contact

In this section, we defined the virtual operator and virtual environment models based on (3). The parameters of virtual operator and environment models are set as $\boldsymbol{D}_h = \text{daig}(10, 10, 10)$, $\boldsymbol{S}_h = \text{daig}(100, 100, 100)$, $\boldsymbol{D}_e = \text{daig}(15, 15, 15)$, and $\boldsymbol{S}_e = \text{daig}(100, 100, 100)$, where the magnitude of the parameter on torque is mN. Furthermore, the extra operator torque $\boldsymbol{f}_h$ is designed as shown in Fig. 17. Our purpose is to employ the virtual operator and environment models to simulate the effects of the operator and environment on the teleoperation system. Real operator is not involved in the system. In this case, the teleoperation system based on these virtual torque models can reach a balanced state with the regulation of the controllers. Moreover, the extra operator torque can achieve the additional action of the operator on the master robot, which can also make the changes in joint position, operator and environment torques. The proposed control scheme is also compared with the controllers in [47] (case 1) and [49] (case 2). Figs. 18–20 show the performance of position and force tracking with proposed control, case1, and case 2, respectively. Among these figures, the blue solid line represents the curves of the position and force of the master robot, and the red dotted line represents the curve of the position and force of the slave robot. Fig. 19 illustrates that control system in case 1 cannot guarantee accurate position synchronization and torque tracking performance under force contact condition. Figs. 18 and 20 show that the system with proposed and case 2 have better tracking performance. However, from the position and force tracking curves after exerting extra operator torques, the proposed finite-time control scheme has the faster convergence speed than the nonfinite-time control method in case 2. The RMSEs of position and force tracking errors in Figs. 18–20 are listed in Table IV. It can also be seen from the RMES values that the proposed control method has better tracking performance of position and force.

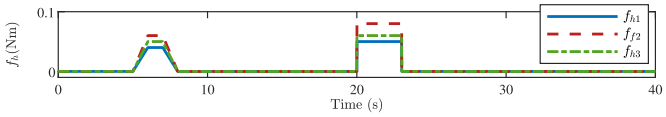

Fig. 17. Virtual operator torque used in the experiment.

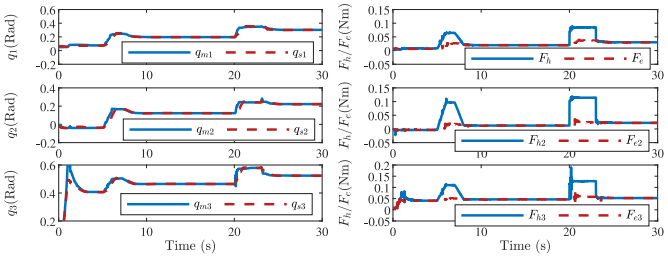

Fig. 18. Position and torque tracking with the proposed control method.

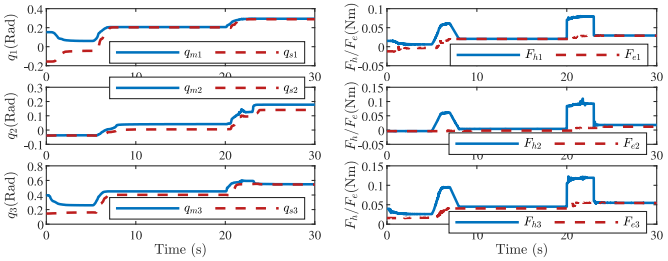

Fig. 19. Position and torque tracking with case 1.

TABLE IV
RMSE OF POSITION AND FORCE TRACKING ERRORS

RMSE	Position tracking			Force tracking		
	Proposed	Case1	Case2	Proposed	Case1	Case2
Joint1	**0.0123**	0.0974	0.0453	**0.0106**	0.0286	0.0266
Joint2	**0.0132**	0.0834	0.0286	**0.0194**	0.0438	0.0403
Joint3	**0.0134**	0.0985	0.0406	**0.0151**	0.0360	0.0322

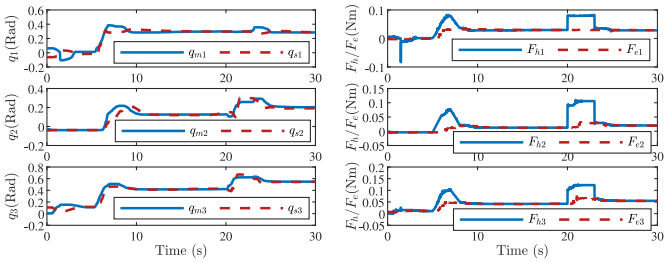

Fig. 20. Position and torque tracking with case 2.

VII. Conclusion

In this article, the position and force tracking control problems for the teleoperation system with time-varying delay and dynamic uncertainties have been investigated. The position and force tracking errors are combined as the error systems for control scheme design. Compared to some existing research work, the proposed control method has the finite-time performance and the acceleration signals do not need to be used. The simulation experiment and practical experiment have been conducted to verify the validity of the proposed control scheme.

Appendix
Young's Inequality and Proof of Lemmas 1 and 2

A. Young's Inequality

Lemma 3: If the positive constants $g, h > 1$ and $(1/g) + (1/h) = 1$, for $\forall e, f \geq 0$, there has the inequality as

$$ef \leq \frac{e^g}{g} + \frac{f^h}{h}.$$

Especially, when $g = h = 2$ and $f = 1$, there has a positive constant p such that

$$e = \frac{e}{p}p \leq \frac{e^2}{2p^2} + \frac{p^2}{2}.$$

B. Proof of Lemma 1

Proof: First, a well-known lemma is introduced to assist the proof

Lemma 4 [55]: For $c_1 > 0$, $c_2 > 0$, and $0 < b < 1$, the following inequality is always established:

$$(c_1 + c_2)^b \leq c_1^b + c_2^b.$$

Obviously, when $c_1 = 0$ or $c_2 = 0$, the above inequality is still holds. For any $a_1, a_2, \ldots, a_k \geq 0$ and $k \leq 2$, we have

$$(a_1 + a_2)^b \leq a_1^b + a_2^b.$$

For $k = 3$, it is apparent that

$$(a_1 + a_2 + a_3)^b \leq a_1^b + a_2^b + a_3^b.$$

We assume that for $k = n$, the inequality in Lemma 1 holds, it has

$$(a_1 + a_2 + a_3 + \cdots + a_n)^b \leq a_1^b + a_2^b + a_3^b + \cdots + a_n^b.$$

Then for $k = n + 1$, we can get that

$$\begin{aligned}&(a_1 + a_2 + a_3 + \cdots + a_n + a_{n+1})^b \\ &\leq (a_1 + a_2 + a_3 + \cdots + a_n)^b + a_{n+1}^b \\ &\leq a_1^b + a_2^b + a_3^b + \cdots + a_n^b + a_{n+1}^b.\end{aligned}$$

Based on the principle of mathematical, it is concluded that Lemma 1 is established for any positive integer n. ■

C. Proof of Lemma 2

Proof: A finite-time stable Lemma is described as follows.

Lemma 5 [63]: Consider the nonlinear system $\dot{x} = f(x)$, $f(0) = 0$, $x \in \mathcal{R}^n$, $x(0) = x_0$, there is a positive continuously differentiable function $V(x)$ defined in a neighborhood $U \subset \mathcal{R}^n$, if $\dot{V}(x) \leq -cV^a(x)$, where $c > 0$ and $0 < a < 1$, the zero solution of the system is finite-time stable. If $U = \mathcal{R}^n$ and $V(x)$ is also radially unbounded, the zero solution is globally finite-time stable.

Furthermore, consider the nonlinear system mentioned above, if the Lyapunov function is satisfied as

$$\dot{V}(x) + \alpha V(x) + \beta V^\sigma(x) \leq 0$$

where $\alpha, \beta > 0$ and $0 < \sigma < 1$.

It is obvious that the finite-time stability of Lyapunov function $V(x)$ can be obtained, and the system is finite-time stable. Define $\dot{V}(x) + \alpha V(x) + \beta V^\sigma(x) = 0$, we have

$$\frac{dV(x)}{dt} = -\alpha V(x) - \beta V^\sigma(x).$$

There has

$$dt = \frac{1}{-\alpha V(x) - \beta V^\sigma(x)} dV(x). \tag{47}$$

Then the setting time T_{set} can be described as

$$\begin{aligned}T_{set} &= \int_{V(x_0)}^{V(x)\to 0} \frac{1}{-\alpha V(x) - \beta V^\sigma(x)} dV(x) \\ &= \frac{1}{\alpha(\sigma - 1)} \ln \beta - \frac{1}{\alpha(\sigma - 1)} \ln\left[\alpha V^{1-\sigma}(x_0) + \beta\right] \\ &= \frac{1}{\alpha(1 - \sigma)} \ln \frac{\alpha V^{1-\sigma}(x_0) + \beta}{\beta}.\end{aligned}$$

Therefore, based on the inequality, the setting time T_{set} has

$$T_{set} \leq \frac{1}{\alpha(1 - \sigma)} \ln \frac{\alpha V^{1-\sigma}(x_0) + \beta}{\beta}.$$

■

Then the proof of Lemmas 1 and 2 are completed.

References

[1] T. Imaida, Y. Yokokohji, T. Doi, M. Oda, and T. Yoshikawa, "Ground-space bilateral teleoperation of ETS-VII robot arm by direct bilateral coupling under 7-s time delay condition," *IEEE Trans. Robot. Autom.*, vol. 20, no. 3, pp. 499–511, Jun. 2004.

[2] S. Soylu, F. Firmani, B. J. Buckham, and R. P. Podhorodeski, "Comprehensive underwater vehicle-manipulator system teleoperation," in *Proc. Oceans Conf.*, Seattle, WA, USA, 2010, pp. 1–8.

[3] C. Lau, R. S. Churchill, J. Kim, F. A. Matsen, and Y. Kim, "Asynchronous Web-based patient-centered home telemedicine system," *IEEE Trans. Biomed. Eng.*, vol. 49, no. 12, pp. 1452–1462, Dec. 2002.

[4] X. B. Guo, A. G. Song, and Y. Zhai, "Neural network control for telerehabilitation robot based on variable gain," in *Proc. Int. Conf. BioMed. Eng. Informat.*, Sanya, China, 2008, pp. 778–782.

[5] P. W. Xiong, X. D. Zhu, A. G. Song, L. Y. Hu, and X. P. P. Liu, "A target grabbing strategy for telerobot based on improved stiffness display device," *IEEE-CAA J. Autom. Sinica*, vol. 4, no. 4, pp. 661–667, Dec. 2016.

[6] P. M. Kebria, H. Abdi, M. M. Dalvand, A. Khosravi, and S. Nahavandi, "Control methods for Internet-based teleoperation systems: A review," *IEEE Trans. Human-Mach. Syst.*, vol. 49, no. 1, pp. 32–46, Feb. 2019.

[7] T. B. Sheridan and W. R. Ferrel, "Remote manipulative control with transmission delay," *IEEE Trans. Human Factors Electron.*, vol. HFE-6, no. 1, pp. 24–32, Sep. 1965.

[8] T. B. Sheridan and W. R. Ferrel, *Telerobotics, Automation, and Human Supervisory Control*. Cambridge, U.K.: MIT Press, 1992.

[9] S. Lee, G. Bekey, and A. Bejczy, "Computer control of space-borne teleoperators with sensory feedback," in *Proc. IEEE Int. Conf. Robot. Autom.*, St. Louis, MO, USA, 1985, pp. 205–214.

[10] L. P. Chan, F. Naghdy, and D. Stirling, "Application of adaptive controllers in teleoperation systems: A survey," *IEEE Trans. Human-Mach. Syst.*, vol. 44, no. 3, pp. 337–352, Jun. 2014.

[11] R. Ortega, Z. P. Jiang, and D. J. Hill, "Passivity-based control of nonlinear systems: A tutorial," in *Proc. Amer. Control Conf.*, vol. 5. Albuquerque, NM, USA, 1997, pp. 2633–2637.

[12] R. J. Anderson and M. W. Spong, "Bilateral control of teleoperators with time delay," *IEEE Trans. Autom. Control*, vol. 34, no. 5, pp. 494–501, May 1989.

[13] H. H. Chen and L. Y. Chen, "Passivity-based control framework for task-space bilateral teleoperation with parametric uncertainty over unreliable networks," *ISA Trans.*, vol. 70, pp. 187–199, Sep. 2017.

[14] G. Niemeyer and J.-J. E. Slotine, "Stable adaptive teleoperation," *IEEE J. Ocean. Eng.*, vol. 16, no. 1, pp. 152–162, Jan. 1991.

[15] S. Munir and W. J. Book, "Internet-based teleoperation using wave variables with prediction," *IEEE/ASME Trans. Mechatronics*, vol. 7, no. 2, pp. 124–133, Jun. 2002.

[16] Z. Chen, F. H. Huang, W. Song, and S. Q. Zhu, "A novel wave-variable based time-delay compensated four-channel control design for multilateral teleoperation system," *IEEE Access*, vol. 6, pp. 25506–25516, 2018.

[17] E. Slawinski and V. Mut, "PD-like controllers for delayed bilateral teleoperation of manipulators robots," *Int. J. Robust Nonlinear Control*, vol. 25, no. 12, pp. 1801–1815, Aug. 2015.

[18] C.-C. Hua, X. Yang, J. Yan, and X.-P. Guan, "On exploring the domain of attraction for bilateral teleoperator subject to interval delay and saturated P + d control scheme," *IEEE Trans. Autom. Control*, vol. 62, no. 6, pp. 2923–2928, Jun. 2017.

[19] H. C. Cho, J. H. Park, K. Kim, and J. O. Park, "Sliding-mode-based impedance controller for bilateral teleoperation under varying time-delay," in *Proc. IEEE Int. Conf. Robot. Autom.*, Seoul, South Korea, 2001, pp. 1025–1030.

[20] S. A. Wais, S. Khoo, T. H. Lee, L. Shanmugam, and S. Nahavandi, "Robust H_∞ cost guaranteed integral sliding mode control for the synchronization problem of nonlinear tele-operation system with variable time-delay," *ISA Trans.*, vol. 72, pp. 25–36, Jan. 2018

[21] Y. N. Yang, C. C. Hua, J. P. Li, and X. P. Guan, "Finite-time output-feedback synchronization control for bilateral teleoperation system via neural networks," *Inf. Sci.*, vols. 406–407, pp. 216–233, Sep. 2017.

[22] Z. J. Li, X. Q. Cao, and N. Ding, "Adaptive fuzzy control for synchronization of nonlinear teleoperators with stochastic time-varying communication delays," *IEEE Trans. Fuzzy Syst.*, vol. 19, no. 4, pp. 745–757, Aug. 2011.

[23] D. Sun, Q. F. Liao, and H. L. Ren, "Type-2 fuzzy modeling and control for bilateral teleoperation system with dynamic uncertainties and time-varying delays," *IEEE Trans. Ind. Electron.*, vol. 65, no. 1, pp. 447–459, Jan. 2018.

[24] Y. N. Yang, C. Ge, H. Wang, X. Y. Li, and C. C. Hua, "Adaptive neural network based prescribed performance control for teleoperation system under input saturation," *J. Franklin Inst.*, vol. 352, no. 5, pp. 1850–1866, May 2015.

[25] C. G. Yang, X. J. Wang, Z. J. Li, Y. A. Li, and C.-Y. Su, "Teleoperation control based on combination of wave variable and neural networks," *IEEE Trans. Syst., Man, Cybern., Syst.*, vol. 47, no. 8, pp. 2125–2136, Aug. 2017.

[26] H. Q. Wang, P. X. Liu, and S. C. Liu, "Adaptive neural synchronization control for bilateral teleoperation systems with time delay and backlash-like hysteresis," *IEEE Trans. Cybern.*, vol. 47, no. 10, pp. 3018–3026, Oct. 2017.

[27] F. H. Huang, W. Zhang, Z. Chen, J. Z. Tang, W. Song, and S. Q. Zhu, "RBFNN-based adaptive sliding mode control design for nonlinear bilateral teleoperation system under time-varying delays," *IEEE Access*, vol. 7, pp. 11905–11912, 2019.

[28] L. Yang, K. R. Chen, and Z. F. Xu, "Adaptive tracking control of a nonlinear teleoperation system with uncertainties in kinematics and dynamics," *Adv. Mech. Eng.*, vol. 11, no. 4, pp. 1–10, Apr. 2019.

[29] Y. C. Liu and M. H. Khong, "Adaptive control for nonlinear teleoperators with uncertain kinematics and dynamics," *IEEE/ASME Trans. Mechatronics*, vol. 20, no. 5, pp. 2550–2562, Oct. 2015.

[30] Z. Chen, B. Liang, T. Zhang, X. Wang, and B. Zhang, "Adaptive bilateral control for nonlinear uncertain teleoperation with guaranteed transient performance," *Robotica*, vol. 34, no. 10, pp. 2205–2222, Oct. 2016.

[31] Y. Li, K. Li, and S. Tong, "Finite-time adaptive fuzzy output feedback dynamic surface control for MIMO nonstrict feedback systems," *IEEE Trans. Fuzzy Syst.*, vol. 27, no. 1, pp. 96–110, Jan. 2019.

[32] H. Wang, P. X. Liu, X. Zhao, and X. Liu, "Adaptive fuzzy finite-time control of nonlinear systems with actuator faults," *IEEE Trans. Cybern.*, vol. 50, no. 5, pp. 1786–1797, May 2020.

[33] Y. Li, T. Yang, and S. Tong, "Adaptive neural networks finite-time optimal control for a class of nonlinear systems," *IEEE Trans. Neural Netw. Learn. Syst.*, early access, Dec. 19, 2019, doi: 10.1109/TNNLS.2019.2955438.

[34] X. Zhao, X. Wang, S. Zhang, and G. Zong, "Adaptive neural backstepping control design for a class of nonsmooth nonlinear systems," *IEEE Trans. Syst., Man, Cybern., Syst.*, vol. 49, no. 9, pp. 1820–1831, Sep. 2019.

[35] H. Wang, S. Liu, and X. Yang, "Adaptive neural control for non-strict-feedback nonlinear systems with input delay," *Inf. Sci.*, vol. 513, pp. 605–616, Apr. 2020.

[36] L. Ma, X. Huo, X. Zhao, B. Niu, and G. Zong, "Adaptive neural control for switched nonlinear systems with unknown backlash-like hysteresis and output dead-zone," *Neurocomputing*, vol. 357, no. 10, pp. 203–214, Sep. 2019.

[37] Y. Li, K. Li, and S. Tong, "Adaptive neural network finite-time control for multi-input and multi-output nonlinear systems with positive powers of odd rational numbers," *IEEE Trans. Neural Netw. Learn. Syst.*, vol. 31, no. 7, pp. 2532–2543, Jul. 2020.

[38] D.-H. Zhai and Y. Q. Xia, "Adaptive control of semi-autonomous teleoperation system with asymmetric time-varying delays and input uncertainties," *IEEE Trans. Cybern.*, vol. 47, no. 11, pp. 3621–3633, Nov. 2017.

[39] Y. N. Yang, C. C. Hua, and X. P. Guan, "Adaptive fuzzy finite-time coordination control for networked nonlinear bilateral teleoperation system," *IEEE Trans. Fuzzy Syst.*, vol. 22, no. 3, pp. 631–641, Jun. 2014.

[40] D.-H. Zhai and Y. Q. Xia, "Finite-time control of teleoperation systems with input saturation and varying time delays," *IEEE Trans. Syst., Man, Cybern., Syst.*, vol. 47, no. 7, pp. 1522–1534, Jul. 2017.

[41] Y. N. Yang, C. C. Hua, and X. P. Guan, "Finite-time synchronization control for bilateral teleoperation under communication delays," *Robot. Comput. Integr. Manuf.*, vol. 31, pp. 61–69, Feb. 2015.

[42] Y. N. Yang, C. C. Hua, and X. P. Guan, "Finite time control design for bilateral teleoperation system with position synchronization error constrained," *IEEE Trans. Cybern.*, vol. 46, no. 3, pp. 609–619, Mar. 2016.

[43] Z. W. Wang, Z. Chen, B. Liang, and B. Zhang, "A novel adaptive finite time controller for bilateral teleoperation system," *Acta Astronautica*, vol. 144, pp. 263–270, Mar. 2018.

[44] H. C. Zhang, A. G. Song, and S. B. Shen, "Adaptive finite-time synchronization control for teleoperation system with varying time delays," *IEEE Access*, vol. 6, pp. 40940–40949, 2018.

[45] Z. W. Wang, Z. Chen, Y. M. Zhang, X. Y. Yu, X. Wang, and B. Liang, "Adaptive finite-time control for bilateral teleoperation systems with jittering time delays," *Int. J. Robust Nonlinear Control*, vol. 29, no. 4, pp. 1007–1030, Mar. 2019.

[46] F. Hashemzadeh and M. Tavakoli, "Position and force tracking in nonlinear teleoperation systems under varying delays," *Robotica*, vol. 33, no. 4, pp. 1003–1016, May 2015.

[47] S. Ganjefar, S. Rezaei, and F. Hashemzadeh, "Position and force tracking in nonlinear teleoperation systems with sandwich linearity in actuators and time-varying delay," *Mech. Syst. Signal Process.*, vol. 86, pp. 308–324, Mar. 2017.

[48] V. Chawda and M. K. O'Malley, "Position synchronization in bilateral teleoperation under time-varying communication delays," *IEEE/ASME Trans. Mechatronics*, vol. 20, no. 1, pp. 245–253, Feb. 2015.

[49] H. C. Zhang, A. G. Song, and H. J. Li, "Adaptive position and force tracking control in teleoperation system with time-varying delays," in *Proc. Int. Conf. Intell. Robot. Appl.*, 2019, pp. 613–624.

[50] H. Amini, S. M. Rezaei, M. Zareinejad, and H. Ghafarirad, "Enhanced time delayed linear bilateral teleoperation system by external force estimation," *Trans. Inst. Meas. Control*, vol. 35, no. 5, pp. 637–647, Jul. 2013.
[51] L. P. Chan, F. Naghdy, and D. Stirling, "Position and force tracking for non-linear haptic telemanipulator under varying delays with an improved extended active observer," *Robot. Auton. Syst.*, vol. 75, pp. 145–160, Jan. 2016.
[52] F. Azimifar, M. Abrishamkar, B. Farzaneh, A. A. D. Sarhan, and H. Amini, "Improving teleoperation system performance in the presence of estimated external force," *Robot. Comput. Integr. Manuf.*, vol. 46, pp. 86–93, Aug. 2017.
[53] D. Sun, Q. F. Liao, T. Stoyanov, A. Kiselev, and A. Loutfi, "Bilateral telerobotic system using Type-2 fuzzy neural network based moving horizon estimation force observer for enhancement of environmental force compliance and human perception," *Automatica*, vol. 106, pp. 358–373, Aug. 2019.
[54] Y. Yuan, Y. J. Wang, and L. Guo, "Force reflecting control for bilateral teleoperation system under time-varying delays," *IEEE Trans. Ind. Informat.*, vol. 15, no. 2, pp. 1162–1172, Feb. 2019.
[55] H. J. Li and A. G. Song, "Virtual-environment modeling and correction for force-reflecting teleoperation with time delay," *IEEE Trans. Ind. Electron.*, vol. 54, no. 2, pp. 1227–1233, Apr. 2007.
[56] X. N. Xu, A. G. Song, D. J. Ni, H. J. Li, P. W. Xiong, and C. C. Zhu, "Visual-haptic aid teleoperation based on 3-D environment modeling and updating," *IEEE Trans. Ind. Electron.*, vol. 63, no. 10, pp. 6419–6428, Oct. 2016.
[57] P. Arcara and C. Melchiorri, "Control schemes for teleoperation with time delay: A comparative study," *Robot. Auton. Syst.*, vol. 38, no. 1, pp. 49–64, Jan. 2002.
[58] A. J. Kurdila, F. J. Narcowich, and J. D. Ward, "Persistency of excitation in identification using radial basis function approximants," *SIAM J. Control Optim.*, vol. 33, no. 2, pp. 625–642, Mar. 1995.
[59] Z. Zhu, Y. Q. Xia, and M. Y. Fu, "Attitude stabilization of rigid spacecraft with finite-time convergence," *Int. J. Robust Nonlinear Control*, vol. 21, no. 6, pp. 686–702, 2011.
[60] S. H. Yu, X. H. Yu, B. Shirinzadeh, and Z. H. Man, "Continuous finite-time control for robotic manipulators with terminal sliding mode," *Automatica*, vol. 41, no. 11, pp. 1957–1964, 2005.
[61] H. K. Khalil, *Nonlinear Systems*, 3rd ed. Upper Saddle River, NJ, USA: Prentice-Hall, 2002.
[62] Z. Li, Y. Xia, and C. Y. Su, *Intelligent Networked Teleoperation Control*. Berlin, Germany: Springer-Verlag, 2015.
[63] Y. Hong, J. Huang, and Y. S. Xu, "On an output feedback finite-time stabilization problem," *IEEE Trans. Autom. Control*, vol. 46, no. 2, pp. 305–309, Feb. 2001.

Haochen Zhang received the B.S. degree in automatic from Northeastern University, Shenyang, China, in 2009, and the M.S. degree in control theory and control engineering form the Lanzhou University of Technology, Lanzhou, China, in 2013. He is currently pursuing the Ph.D. degree with the School of Instrument Science and Engineering, Southeast University, Nanjing, China.

He is also currently a Lecturer with the College of Electrical and Information Engineering, Lanzhou University of Technology. His current research interests are teleoperation control and robot control.

Aiguo Song (Senior Member, IEEE) received the B.S. degree in automatic control and the M.S. degree in measurement and control from the Nanjing University of Aeronautics and Astronautics, Nanjing, China, 1990 and 1993, respectively, and the Ph.D. degree in measurement and control from Southeast University, Nanjing, in 1998.

From 1998 to 2000, he was an Associate Professor with the Department of Instrument Science and Engineering, Southeast University, where he was the Director of the Robot Sensor and Control Laboratory from 2000 to 2003. He is currently a Professor with the School of Instrument Science and Engineering, Southeast University. His major interests concentrate on teleoperation control, haptic display, Internet telerobotics, and distributed measurement systems.

Huijun Li received the B.S. degree in instrument science and the M.S. degree in condensed matter physics from Zhengzhou University, Zhengzhou, China, in 1999 and 2002, respectively, and the Ph.D. degree in measurement and control from Southeast University, Nanjing, China, in 2005.

She is currently an Associate Researcher with the Department of Instrument Science and Engineering, Southeast University. Her current interests include teleoperation and rehabilitation robotics.

Dapeng Chen (Member, IEEE) received the B.S. degree in electrical engineering and automation from the Anhui University of Science and Technology, Huainan, China, in 2011, and the Ph.D. degree in instrumentation science and technology from Southeast University, Nanjing, China, in 2019.

He was a Visiting Scholar with the Intelligent, Multimedia, and Interactive Systems Lab, University of North Carolina at Charlotte, Charlotte, NC, USA, from 2016 to 2017. He is currently a Lecturer with the School of Automation, Nanjing University of Information Science and Technology, Nanjing. His research interests include haptic display, haptic device, and human–computer interaction.

Liqiang Fan received the B.S. degree in automatic from the Nanjing University of Information Science and Technology, Nanjing, China, in 2012, and the M.S. degree in control theory and control engineering form Hohai University, Nanjing, in 2016. He is currently pursuing the Ph.D. degree with the School of Instrument Science and Engineering, Southeast University, Nanjing.

His current research interests are haptic interface and force feedback.